Silent cold-sensing neurons contribute to cold allodynia in neuropathic pain

Donald Iain MacDonald, Ana P. Luiz, Federico Iseppon, Queensta Millet, Edward C. Emery and John N. Wood

Abstract

Neuropathic pain patients often experience innocuous cooling as excruciating pain. The cell and molecular basis of this cold allodynia is little understood. We used *in vivo* calcium imaging of sensory ganglia to investigate how the activity of peripheral cold-sensing neurons was altered in three mouse models of neuropathic pain: oxaliplatin-induced neuropathy, partial sciatic nerve ligation and ciguatera poisoning. In control mice, cold-sensing neurons were few in number and small in size. In neuropathic animals with cold allodynia, a set of normally silent large-diameter neurons became sensitive to cooling. Many of these silent cold-sensing neurons responded to noxious mechanical stimuli and expressed the nociceptor markers $Na_V1.8$ and CGRPα. Ablating neurons expressing $Na_V1.8$ resulted in diminished cold allodynia. The silent cold-sensing neurons could also be activated by cooling in control mice through blockade of K_V1 voltage-gated potassium channels. Thus silent cold-sensing neurons are unmasked in diverse neuropathic pain states and cold allodynia results from peripheral sensitization caused by altered nociceptor excitability.

Author affiliation:

Molecular Nociception Group, Wolfson Institute for Biomedical Research, University College London, Gower Street, WC1E 6BT, London, UK

Correspondence to: John N. Wood

Molecular Nociception Group, Wolfson Institute for Biomedical Research, University College London, Gower Street, WC1E 6BT, London, UK

E-mail: j.wood@ucl.ac.uk

Running title: Silent cold neurons drive cold allodynia

Keywords: pain; cold allodynia; neuropathic pain; potassium channels; sodium channels

Introduction

Chronic pain patients suffering from cold allodynia experience normally innocuous cooling as excruciating pain (Jensen and Finnerup, 2014). Cold allodynia is a common symptom of neuropathic pain caused by chemotherapy, nerve injury or ciguatera poisoning, with a prevalence of up to 90% (Yin *et al.*, 2015; MacDonald *et al.*, 2020). How do neuropathic pain conditions with different etiologies give rise to the same sensory disturbance of cold-evoked pain? Despite advances in our understanding of cold sensation, the pathophysiological mechanisms underlying cold allodynia remain elusive.

In the healthy state, peripheral sensory neurons show modality-specific responses to cold, with 'labelled lines' for both mild and extreme cooling (Knowlton *et al.*, 2013; Pogorzala *et al.*, 2013; Emery *et al.*, 2016; Yarmolinsky *et al.*, 2016; Wang *et al.*, 2018; Viana and Voets, 2019). Cold detection involves cooling-gated ion channels like Trpm8, as well as sodium and potassium channels that control excitability at low temperatures (Bautista *et al.*, 2007; Colburn *et al.*, 2007; Dhaka *et al.*, 2007; Zimmermann *et al.*, 2007; Madrid *et al.*, 2009; Morenilla-Palao *et al.*, 2014; Lolignier *et al.*, 2015; Luiz *et al.*, 2019). Mouse knockout studies suggest cold allodynia requires TRP channels and potassium channels expressed by unmyelinated C fibres (Alloui *et al.*, 2006; Colburn *et al.*, 2007; Noël *et al.*, 2009; Descoeur *et al.*, 2011; Nassini *et al.*, 2011; Vetter *et al.*, 2012; Knowlton *et al.*, 2013; Pereira *et al.*, 2014; González *et al.*, 2017). A role for sodium channels enriched in A fibres is also evident, however (Sittl *et al.*, 2012; Vetter *et al.*, 2012; Deuis *et al.*, 2013; Inserra *et al.*, 2017). Mechanistic investigation of the cells and molecules driving cold allodynia has proved difficult because of the challenge in recording large numbers of cold-responsive afferents, as well as the limitations of cold pain behaviour tests (Mckemy, 2010).

To investigate directly if cold allodynia results from plasticity in peripheral sensory neurons, we used *in vivo* calcium imaging to explore how the activity of cold-sensing neurons is altered in neuropathic pain. Here we identify a previously undescribed set of large-diameter silent cold-sensing neurons that contribute to cold allodynia in diverse neuropathic pain states and provide evidence for a potential role of K_V1 potassium channels in unmasking their latent cold sensitivity.

Materials and Methods

Animals

All animal procedures were approved by UCL ethical review committees and were discussed with Home Office inspectors to conform to UK Home Office regulations under Project licence P413329A2. Mouse lines used in this study are summarized in **Supplementary Table 1**.

All mouse lines were maintained on a C57/BL6 background and breeding strategies are as previously reported (Akopian *et al.*, 1999; Abrahamsen *et al.*, 2008; Minett *et al.*, 2012; Emery *et al.*, 2016; Luiz *et al.*, 2019). Cre-dependent tdTomato reporter mice expressing GCaMP3 were generated by crossing subset-specific Cre mice with animals homozygous for Rosa-flox-stop tdTomato and homozygous for Pirt-GCaMP3. $Na_V1.8$-Cre-dependent tdTomato and diphtheria toxin mice expressing GCaMP3 were generated by crossing $Na_V1.8$ Cre mice with animals heterozygous for Rosa-flox-stop tdTomato, heterozygous Rosa-flox-stop DTA and homozygous for Pirt-GCaMP3.

Both male and female (>6 weeks) mice were used for all experiments, and the number of mice of each sex used to generate each dataset is reported in **Supplementary Table 2**. The investigator was blinded to treatment and/or genotype. For genotyping, genomic DNA was isolated from ear biopsy for PCR. Genotyping primers are listed in **Supplementary Table 3**.

Tamoxifen treatment

CGRPα-CreERT2 mice were given three 200 µl doses of a 1% tamoxifen solution on consecutive days between 6-8 weeks of age. TrkB-CreERT2 mice were given five 200 µl doses of a 1% tamoxifen solution on consecutive days between 8-10 weeks of age. Tamoxifen was made-up in a 15% ethanol/85% sunflower oil.

Neuropathic pain models

Standard behavioural tests were used to assess neuropathic pain and are described in detail in the **Supplementary Methods**. Animals were acclimatized to handling to minimize stress during the testing. All behavioural experiments were performed at a room temperature of 18 to 21°C.

Oxaliplatin:

Chemotherapy-induced neuropathy was induced in mice by intraplantar injection of oxaliplatin into the left hindpaw (Deuis *et al.*, 2013). Oxaliplatin was made up to a dose of 80 µg in 40 µl of 5% glucose solution, due to its instability in chloride-containing saline solution. Behavioural testing or imaging was assessed at least 3 hours after injection.

Partial Sciatic Nerve Injury:

Peripheral nerve injury was studied in mice using a modified version of the Seltzer model (Seltzer *et al.*, 1990). Surgical procedures were performed under isoflurane anaesthesia (2–3%). After the left thigh area was shaved and the skin sterilized with 70% ethanol, a longitudinal skin incision was made at the level of the femur. With the help of forceps, the muscle fibres were separated to allow visualization of the sciatic nerve. The partial nerve injury was induced by tying a tight ligature with 6-0 silk suture around approximately 1/3 of the diameter of the sciatic nerve. The skin was then closed with 6-0 Vicril suture and animals kept in a warm enclosure until complete recovery. Behavioural testing was performed at 2 and 4 weeks post-surgery, and imaging experiments were carried out between 4 and 5 weeks after surgery.

Ciguatoxin-2:

Ciguatoxin-2 (P-CTX-2) was a gift from Richard Lewis (University of Queensland). Because P-CTX-2 is highly lipophilic and sticks to plastic surfaces, it was made up to 10 µM in 50% methanol solution, stored in a glass vial at -20°C and aliquoted using a metal/glass Hamilton syringe. The stock solution was diluted in saline containing 1% BSA to produce a final concentration of 100nM. Mice undergoing imaging or behavioural testing were injected intraplantar with 20 µl of 100nM P-CTX-2, and the effect of the drug measured after 20-30 minutes (Vetter *et al.*, 2012).

In Vivo Calcium Imaging

Acquisition:

Mice expressing GCaMP3 were anesthetized using ketamine (100 mg/kg), xylazine (15 mg/kg) and acepromazine (2.5 mg/kg). Depth of anaesthesia was confirmed by pedal reflex and breathing rate. Animals were maintained at a constant body temperature of 37°C using a heated mat (VetTech). Lateral laminectomy was performed at spinal level L3-5. In brief, the skin was incised longitudinally, and the paravertebral muscles were cut to expose the vertebral column. Transverse and superior articular processes of the vertebra were removed using microdissection scissors and OmniDrill 35 (WPI). To obtain a clear image of the sensory neuron cell bodies in the ipsilateral dorsal root ganglion (DRG), the dura mater and the arachnoid membranes were carefully opened using microdissection forceps. The animal was mounted onto a custom-made clamp attached to the vertebral column (L1), rostral to the laminectomy. The trunk of the animal was slightly elevated to minimize interference caused by respiration. Artificial cerebrospinal fluid [containing 120 mM NaCl, 3 mM KCl, 1.1 mM $CaCl_2$, 10 mM glucose, 0.6 mM NaH_2PO_4, 0.8 mM $MgSO_4$, 1.8 mM $NaHCO_3$ (pH 7.4) with NaOH] was perfused over the exposed DRG during the procedure to maintain tissue integrity, or the DRG was isolated by coating with silicone elastomer.

Images were acquired using a Leica SP8 confocal microscope. A 10x dry, 0.4-N.A. objective with 2.2 mm working distanced was used, with image magnification of 0.75-3x optical zoom. GCaMP3 was excited using a 488 nm laser line (1-15% laser power). tdTomato was excited using a 552 nm laser line (1-15% laser power). Filtering and collection of the emission light was optimized to maximize yield and minimize cross-talk (Leica Dye 164 Finer, LasX software, Leica). GCaMP was detected using a hybrid detector (100% gain) and tdTomato using a photomultiplier tube (500-600V gain). 512 x 512 pixel images were captured at a frame rate of 1.55 Hz, bidirectional scan speed of 800 Hz, and pixel dwell time of 2.44 µs.

Noxious and innocuous stimuli were applied to the left hindpaw, ipsilateral to the exposed DRG. Thermal stimuli were applied by a Peltier-controlled thermode, or by immersion of the paw in ice-water (nominally 0°C), acetone (100%) or 55°C water using a Pasteur pipette. Mechanical stimuli were noxious pinch with serrated forceps, and innocuous brushing with a small paint-brush (ProArte-2) or cotton-swab. An interval of at least 30 s separated each stimulus application. Pharmacological agents were delivered by intraplantar injection and are summarized in **Supplementary Table 4**.

Image analysis:

Image stacks were registered to a reference frame using the FIJI plugin TurboReg (accurate rigid body transformation) to correct for XY drift. Stacks with excessive Z movement were excluded from analysis. Regions of interest (ROI) were manually drawn around responding cells using the free hand tool in FIJI. The time series of mean pixel intensity for each ROI was extracted and smoothened by a four time point moving average to remove high-frequency noise. Next, we calculated the derivative of the mean pixel intensity. Neurons were classed as responders if, within 30 s of stimulus application, the maximum derivative was greater than the baseline (10 s preceding stimulus application) derivative plus five standard deviations – that is, a Z-score of at least 5. We then calculated the $\Delta F/F_0$ value for each response to obtain a normalized measure of change in fluorescence. Neurons which showed a $\Delta F/F_0$ less than 0.25 were then discarded. Each trace was then manually screened as a further precaution against false positives. The remaining neurons that made up the responding population were then used for statistical analysis. Cross-sectional area for each ROI in μm^2 was also measured.

The red channel of the reference image was used determine whether a cell was positive for tdTomato. Five regions of interest were drawn in background areas of the image negative for tdTomato and average pixel intensity measured to calculate the mean and standard deviation of the background red fluorescence. Red fluorescence in responding cells was Z-scored versus the background value, and cells were counted as tdTomato positive if the Z-score was greater than 5.

Quantification and Statistical Analysis

For *in vivo* imaging experiments, n refers to the number of cells responding to any stimulus. For electrophysiology experiments, n refers to the number of recorded cells. For all imaging and physiology data, the number of animals used is indicated in the legend. For behavioural experiments, n refers to the number of animals.

Datasets are presented using appropriate summary statistics as indicated in the legend. For behavioural data, error bars denote mean ± 95% confidence interval, unless otherwise indicated. For *in vivo* imaging experiments, cells from all animals were pooled for analysis. These non-parametric data are summarized using medians with quartiles, or cumulative probability plots.

For categorical data, 95% confidence intervals around proportions were estimated using the Wilson-Brown method.

Tests of statistical comparison for each dataset are described in figure legends. All test statistics are summarized in detail in **Supplementary Table 5** for the main figures and in **Supplementary Table 6** for the supplementary figures. When comparing two groups, unpaired *t* test or Mann-Whitney test was used. When comparing the distribution of cell cross-sectional areas for two groups, the Kolmogorov-Smirnov test was used. For more than two groups, One-Way ANOVA or Kruskall-Wallis test was used with post-hoc tests corrected for multiple comparisons. When comparing the effect of two factors on multiple groups, a repeated-measures Two-Way ANOVA was used, with post-hoc tests corrected for multiple comparisons. For categorical data, proportions were compared using χ^2 test. Curve fitting was performed using linear regression or non-linear regression functions.

Statistical tests were all performed using GraphPad Prism 7. Differences were considered significant where $p<0.05$.

Data availability

Data is available at https://doi.org/10.6084/m9.figshare.13293050

Results

Silent cold-sensing neurons are unmasked during chemotherapy-induced neuropathy

To investigate the mechanisms of cold allodynia, we used *in vivo* calcium imaging to explore how sensory neuron responses to cooling are altered during chemotherapy-induced neuropathy. Pirt-GCaMP3 mice expressing GCaMP3 in all sensory neurons were treated with oxaliplatin (80 µg/40 µl by hindpaw intraplantar injection). Three hours after injection, both male and female mice displayed extreme cold hypersensitivity, as measured by the number of nociceptive and nocifensive behaviours when the animal was placed on a 5 °C Cold Plate (**Fig. 1A** &

Supplementary Fig. 1A). Oxaliplatin-treated mice also developed mechanical hypersensitivity, but not heat hyperalgesia. The short-latency cold hypersensitivity observed after a single clinical dose of oxaliplatin (~3mg/kg) in this model mimics the rapid onset of cold allodynia in patients (Deuis *et al.*, 2013).

Using laser-scanning confocal microscopy, we imaged cold-evoked calcium signals in sensory neuron somata of L4 dorsal root ganglia from oxaliplatin- and vehicle-treated animals. There was a dramatic change in the peripheral representation of cold following oxaliplatin treatment (**Fig. 1B**). In vehicle-treated mice, neurons responding to either ice-water or acetone were sparse and had small cross-sectional areas, with a mean value of 214.9 μm^2 (**Fig. 1Ci**). In oxaliplatin-treated animals, small cells still responded to cold, however a novel, usually cold-insensitive population of large neurons also became activated by cooling. We consequently divided cold-sensing neurons from the oxaliplatin-treated group into a basal population (within three standard deviations of the vehicle mean cross-sectional area), and an unmasked population (greater than three standard deviations away from this mean, >446.77 µm2) (**Fig. 1Ci & Supplementary Fig. 1B**). Because large neurons normally never respond to cooling, but gain a *de novo* sensitivity to cold following oxaliplatin, we named them 'silent cold-sensing neurons.' The percentage of cells classified as silent cold-sensing neurons rose from 1% (4/383) in vehicle- to 19% (102/542) in oxaliplatin-treated animals (**Fig. 1Cii**).

Interestingly, the response of many silent cold-sensing neurons to acetone continued for tens of seconds beyond the initial delivery of the stimulus (**Fig. 1B**). Consistent with this, oxaliplatin-treated animals show prolonged nocifensive behaviour localized to the ipsilateral paw following acetone application (**Supplementary Fig. 1C**).

Cold allodynia could result from neurons signalling extreme cold becoming active at higher temperatures (González *et al.*, 2017). However, oxaliplatin did not affect thermal activation thresholds of basal cold-sensing neurons, when the hindpaw was stimulated with temperature drops delivered by a Peltier-controlled thermode (**Fig. 1D**). When we quantified peak fluorescence intensity in response to cold as a surrogate for excitability, cold-evoked fluorescence intensity in both the basal and silent populations in the oxaliplatin group was no different to vehicle (**Supplementary Fig. 1D**). These data indicate oxaliplatin does not markedly affect the activation thresholds or excitability of the basally-active cold-sensing neurons.

What effect did oxaliplatin have on neurons responding to other sensory modalities? Cross-sectional area of mechanically-sensitive neurons was unchanged, but heat-activated cells showed a minor shift towards larger cells (**Supplementary Fig. 1B**). There was no increase in the proportion of heat- or mechanically-sensitive cells (**Supplementary Fig. 1E**). Mechanical response magnitude was not altered, although the response to heat was reduced (**Supplementary Fig. 1F**). Thus oxaliplatin treatment results in a modality-specific expansion in the peripheral representation of cold through the recruitment of silent cold-sensing neurons.

We previously showed that nociceptor polymodality is enhanced by inflammatory mediators (Emery *et al.*, 2016). Interestingly, oxaliplatin increased the proportion of mechano-heat neurons from 19% (26/136) to 32% (61/193) (**Supplementary Fig. 1G**). However, few cold-sensing neurons responded to heat (**Fig. 1Ei**). By contrast, the fraction of cold-sensing neurons responding to noxious pinching was markedly increased (**Fig. 1Eii**). For ice-water, this rose from 16% (8/51) to 33% (27/81) and for acetone from 12% (7/58) to 37% (53/145). This is likely an under-estimate because pinching targets a smaller receptive field than ice-water or acetone. These mechano-cold neurons were mainly large-diameter silent cold-sensing neurons (**Fig. 1Eiii** & **Supplementary Fig. 1H**).

Importantly, silent cold-sensing neurons rarely responded to intermediate or low-threshold mechanical stimuli. Only 8% (15/199) of silent cold-sensing neurons responded to repeated stimulation with a 2g Von Frey hair (**Supplementary Fig. 2A&B**). From 48 silent cold-sensing neurons tested, not one responded to stroking the glabrous or hairy skin using a paint-brush or cotton swab (**Supplementary Fig. 2C&D**). The mechanically-sensitive subpopulation of silent cold-sensing neurons therefore primarily respond to high-threshold mechanical stimuli, consistent with a functional identity as nociceptors.

Silent cold-sensing neurons are unmasked during peripheral nerve injury

Are silent cold-sensing neurons unmasked in other neuropathies? To mimic nerve injury-induced neuropathic pain, we performed partial sciatic nerve ligation (PNL) on Pirt-GCaMP3 mice. Two weeks after surgery, nerve injured animals developed mechanical, but not cold, hypersensitivity. At four weeks, we observed a modest cold hypersensitivity using both the acetone and Unilateral Cold Plate test, but no difference in heat nociception. (**Fig. 2A** &

Supplementary Fig. 3A). Qualitatively similar results were obtained in both males and females for all assays (**Supplementary Fig. 3B**).

We therefore imaged both nerve-injured and sham-operated mice between 4 and 5 weeks post-surgery (**Fig. 2B**). In sham-operated mice, cold-sensing neurons were small in size with a mean area of 222.7 μm^2 (**Fig. 2Ci**). After nerve injury, normally cold-insensitive, large-diameter neurons responded to both ice-water and acetone stimuli (**Fig. 2Ci** & **Supplementary Fig. 3C**). Neurons with cross-sectional areas greater than three standard deviations away from the sham mean (>405.4 μm^2) were classified as silent cold-sensing neurons. The silent cold-sensing neuron population expanded from 2% (7/373) to 15% (45/291) (**Fig. 2Cii**). Fewer silent cold-sensing neurons were recruited by nerve injury than oxaliplatin, consistent with a less profound behavioural cold hypersensitivity.

Nerve injury did not alter the thermal activation thresholds of basal cold-sensing neurons (**Fig. 2D**), but the effect on excitability was complex. Acetone-evoked activity was enhanced in the basal population, while silent cells showed reduced responses to ice-water (**Supplementary Fig. 3D**). The number of heat-cold polymodal neurons was unchanged (**Fig. 2Ei**), however the proportion of mechano-cold cells was significantly increased (**Fig. 2Eii**). For ice-water, this rose from 5% (3/64) to 20% (14/71) and for acetone from 0% (0/95) to 10% (7/73). Mechano-cold cells comprised both basal and silent cold-sensing neurons, based on cross-sectional area (**Fig. 2Eiii** & **Supplementary Fig. 3E**). In addition, when the glabrous skin was lightly stroked with a paint-brush, just 2% (1/41) of silent cold-sensing neurons unmasked by nerve injury responded to this low-threshold mechanical stimulus (**Error! Reference source not found.E**). Nerve injury and oxaliplatin thus have broadly similar effects on the peripheral representation of cold, unmasking silent cold-sensing neurons that also sometimes respond to noxious mechanical stimuli.

Neurons responding to other modalities were variably affected by nerve injury. There was no change in cell area for mechanical stimuli, but heat-activated neurons were larger (**Supplementary Fig. 3C**). Significantly more neurons responded to pinch (38% vs. 28%), and there was a trend towards fewer responses to heat (40% vs. 47%) (**Supplementary Fig. 3F**). We saw no difference in the intensity of the response to noxious heat, but pinch-evoked peak activity was decreased (**Supplementary Fig. 3G**). Unlike oxaliplatin, there was no enhancement of mechano-heat polymodality (**Supplementary Fig. 3H**).

Silent cold-sensing neurons are unmasked during ciguatera poisoning

Both oxaliplatin and nerve injury show a delayed onset of cold hypersensitivity. As our imaging preparation is terminal, we could not follow mice in real-time to determine if silent cold-sensing neurons are truly silent in the naive state. To induce cold allodynia within the same imaging session, we turned to a mouse model of ciguatera poisoning, a marine toxin-induced neuropathy characterized by cold pain in the extremities that results from consuming contaminated seafood (Vetter *et al.*, 2012). Hindpaw intraplantar injection of ciguatoxin-2 (P-CTX-2, 100 nM) evoked cold pain by 30 minutes in both male and female mice, as judged by the acetone and 10°C unilateral cold plate test (**Fig. 3A** & **Supplementary Fig. 4A**).

We therefore imaged sensory neuron cold sensitivity over the same time course (**Fig. 3B**). After 30 minutes, P-CTX-2 induced robust responses to cooling in numerous initially cold-insensitive cells (**Fig. 3Ci**). Some neurons actually lost their response to cold, however this was counterbalanced by the large number of cells that gained *de novo* cold sensitivity, resulting in a net expansion of cold population, especially to ice-water. The number of neurons responsive to any cold stimulus rose from 91 to 206 and for ice water went from 69 to 174. P-CTX-2 did not affect how many cells responded to other modalities (**Fig. 3Cii**). Silent cold-sensing neurons unmasked by P-CTX-2 were also large, with a mean cross-sectional area of 820.1 μm^2 (**Fig. 3D**). The size of heat-sensing cells was not markedly altered, although more small neurons responded to noxious pinch (**Supplementary Fig. 4B**).

How did P-CTX-2 treatment affect basally-active cold cells? We quantified the change in threshold of these cells after either P-CTX-2 or vehicle, and saw no difference (**Fig. 3Ei**). Interestingly, P-CTX-2 reduced the peak cold response of these neurons compared to vehicle (**Supplementary Fig. 4C**). Silent cold-sensing neurons showed similar thermal activation thresholds to the basal population (**Fig. 3Eii**), and their activity was not greater (**Supplementary Fig. 4D**). P-CTX-2 did not affect the peak response to other modalities (**Supplementary Fig. 4E**), however there was an increase in the fraction of polymodal mechano-heat neurons from 12% to 25% (**Supplementary Fig. 4F**).

P-CTX-2 increased mechano-cold polymodal neurons responding to ice-water from 4% to 13% (**Fig. 3Fi**). Heat/cold polymodality was also enhanced, albeit not significantly (**Fig. 3Fii**). Interestingly, the proportion of identified silent cold-sensing neurons that responded to noxious mechanical stimuli was at 16% the same in the naïve state and after P-CTX-2. This indicates that at least some silent cold-sensing are responsive to noxious mechanical stimuli before the induction of neuropathy. Few heat/cold cells showed a basal response to heat, indicating heat sensitivity is conferred by P-CTX-2 (**Fig. 3Fiii**). Results were broadly similar when we looked only at the cold-sensing neurons defined by their response to acetone (**Supplementary Fig. 4G**). Finally, cold-sensing neurons unmasked by P-CTX-2 almost never responded to light touch stimuli, either before or after treatment (**Supplementary Fig. 2F**).

These findings demonstrate cold allodynia induced by P-CTX-2 involves unmasking of silent cold-sensing neurons, some of which are pinch-activated mechano-nociceptors. Etiologically-distinct neuropathic pain states therefore give rise to cold pain by a similar mechanism of recruiting cold-insensitive sensory neurons to become cold-responsive.

Molecular characterization of silent cold-sensing neurons that drive cold allodynia in neuropathic pain

What is the molecular identity of silent cold-sensing neurons? We crossed subset-specific Cre or CreERT2 mice with animals harbouring a Cre-dependent tdTomato reporter, on a Pirt-GCaMP3 background. This generated progeny expressing GCaMP3 in all sensory neurons but with tdTomato expression restricted to the cellular subset of interest (**Fig. 4A**). Consequently, we were able to ask if functionally-identified silent cold-sensing neurons express molecular markers labelling major subpopulations of sensory neurons (Usoskin *et al.*, 2014; Zeisel *et al.*, 2018). We focused on oxaliplatin neuropathy because of its ease, reproducibility and clinical relevance. The percentage of neurons responding to any cold stimulus in vehicle and oxaliplatin-treated mice expressing each molecular marker is summarized in **Fig. 4A**, split as before into basal and silent populations.

Ntrk2 (TrkB-CreERT2) is a molecular marker for Aδ-fibre low-threshold mechanoreceptors and was expressed by just 4% of silent cold-sensing neurons (**Fig. 4A**). Silent cold-sensing neurons also showed minimal expression of the Aβ-fibre low-threshold mechanoreceptor marker *Calb*1 (Calb1-Cre) with only 22% overlap (**Fig. 4A**). The molecular profile therefore concurs with the functional data that silent cold-sensing neurons are unlikely to be low-threshold mechanoreceptors, despite their large size. However, silent cold-sensing neurons showed only 30% overlap with *Trpv1* lineage neurons, which encompass a broad mixture of nociceptors and thermosensors (**Fig. 4A**).

Given that some silent cold cells respond to noxious mechanical stimuli, we hypothesized they express *Scn10a*, a marker of mechano-nociceptors (Abrahamsen *et al.*, 2008; von Buchholtz *et al.*, 2020). We previously showed that under physiological conditions the bulk of neurons sensing cold down to 0°C are negative for *Scn10a*, which encodes sodium channel $Na_V1.8$ (Luiz *et al.*, 2019). In agreement with this, very few small-sized cold-sensing neurons were marked by $Na_V1.8$-Cre in animals treated with either vehicle (14%) or oxaliplatin (19%). In contrast, we found 68% of the large-diameter silent cold-sensing neurons unmasked by oxaliplatin expressed $Na_V1.8$ **(Fig. 4A&B**). When we examined animals with cold allodynia evoked by PNL, 52% of silent cold-sensing neurons were marked by $Na_V1.8$, although 41% of smaller cells also expressed $Na_V1.8$ in this model (**Fig. 4C**). Similarly, 55% of the silent cold-sensing neurons unmasked by P-CTX-2 were positive for $Na_V1.8$, with only 11% overlap among the cold cells active in the naïve state (**Fig. 4D**). Thus, in all three neuropathic pain models tested here, most silent cold-sensing neurons express $Na_V1.8$, forming a unique subpopulation of large-diameter *Scn10a*-expressing nociceptors.

To determine which nociceptor subset silent cold-sensing neurons belonged to, we used a Tmem45b-Cre mouse line to identify *Tmem45b*-expressing non-peptidergic nociceptors (Usoskin *et al.*, 2014). Just 5% of silent cold cells in oxaliplatin neuropathy expressed Tmem45b (**Fig. 4A**). On the other hand, 62% of silent cold-sensing neurons in oxaliplatin neuropathy overlapped with *Calca*-expressing peptidergic nociceptors labelled with CGRPα-CreERT2 (**Fig. 4A&E**). The silent cold-sensing neurons also showed substantial overlap with *Calca*-expressing cells in mice with cold allodynia evoked by PNL (57%) or P-CTX-2 (54%), identifying silent cold cells as a set of peptidergic nociceptors commonly involved in cold allodynia (**Fig. 4F&G**). Hence, expression of *Scn10a* or *Calca* can be used to differentiate the silent and basal cold-sensing neurons.

Next, we restricted our analysis only to those silent cold-sensing neurons that were also sensitive to noxious mechanical stimuli, and obtained a similar pattern of marker expression. In the oxaliplatin model, silent cold cells responsive to pinch were strongly positive for *Scn10a* (53%) and *Calca* (68%), but mainly negative for *Trpv1* (27%), with none expressing *Tmem45b*, *Calb1* or *Ntrk2* (**Supplementary Fig. 5A**). In P-CTX-2-treated mice, we also saw that the silent mechanocold neurons largely expressed both *Scn10a* (54%) and *Calca* (83%) (**Supplementary Fig. 5B)**. Thus the mechanosensory subpopulation of silent cold-sensing neurons are also likely peptigdergic nociceptors.

Finally, we used diphtheria toxin to conditionally ablate silent cold-sensing neurons marked by Na$_V$1.8-Cre to test their causal role in cold allodynia (**Fig. 5A**). This ablation encompasses all cells expressing Na$_V$1.8 and is not restricted to silent cold-sensing neurons. Imaging of mice where *Scn10a*-positive nociceptors are ablated shows very few of the large-diameter silent cold-sensing neurons are unmasked by oxaliplatin compared to Na$_V$1.8-Cre mice lacking DTA (**Fig. 5B**). The small basal cold-sensing neurons are retained after killing of *Scn10a*-positive neurons. Although nocifensive behaviour was not fully abolished, we observed a ~50% decrease in oxaliplatin-evoked cold hypersensitivity in Na$_V$1.8-Cre DTA animals (**Fig. 5C**). The molecular identification and subsequent manipulation of silent cold-sensing neurons thus corroborates their causal contribution to cold allodynia in neuropathic pain.

Molecular basis of cold detection by silent cold-sensing neurons

Which sodium channel isoform is required for silent cold-sensing neuron excitability? For mechanistic investigation, we focused on silent cold-sensing neurons responding to ice-water stimuli in the oxaliplatin model. Because Cre is knocked in directly at the Na$_V$1.8 locus, homozygous Na$_V$1.8-Cre mice lack both wild-type *Scn10a* alleles and are thus Na$_V$1.8 nulls without Na$_V$1.8-dependent TTX-resistant voltage-gated sodium currents (**Supplementary Fig. 6B**). When we treated homozygous Na$_V$1.8-Cre mice expressing Cre-dependent tdTomato on a Pirt-GCaMP3 background with oxaliplatin, silent cold-sensing neurons were unmasked (**Fig. 6Ai**). There was no difference between oxaliplatin-treated mice heterozygous or homozygous for Na$_V$1.8-Cre in the cross-sectional areas of cold-responsive cells (**Fig. 6Aii**) or in tdTomato-expression in silent cold-sensing neurons (**Fig. 6Aiii**). Oxaliplatin also evoked cold allodynia in conventional Na$_V$1.8 KO mice (**Supplementary Fig. 6B**). Additionally, imaging of Advillin-Cre conditional Na$_V$1.7 KO mice expressing GCaMP3 revealed recruitment of silent cold-sensing neurons by oxaliplatin (**Fig. 6B**). Thus, pain-related sodium channels Na$_V$1.8 and Na$_V$1.7 are dispensable for silent cold-sensing neuron activity. Treatment of oxaliplatin-injected animals with TTX blocked activity in essentially all basal and silent cold-sensing neurons, however (**Fig. 6C**). 4,9-anhydrousTTX, reported to preferentially inhibit Na$_V$1.6, reduced the number of silent cold-sensing neurons by 57%. The effect of Na$_V$1.6 blockade on basal cold-sensing neurons was comparable to saline (**Fig. 6AC**). Hence, Na$_V$1.6 is likely the predominant sodium channel isoform in silent cold-sensing neurons. When we directly activated sodium channels with the pharmacological potentiator veratridine in naïve mice, we observed no unmasking of large-sized cells; indeed, the activity of cold-sensing neurons was paradoxically reduced (**Fig. 6D**). Activation of sodium channels is therefore not sufficient to induce *de novo* cold sensitivity.

We have previously shown that basally cold-insensitive $Na_V1.8$-positive neurons are enriched with *Kcna1* and *Kcna2*, which encode the voltage-gated potassium channels $K_V1.1$ and $K_V1.2$ (Luiz *et al.*, 2019). These channels are thought to pass a voltage-dependent hyperpolarizing brake current that opposes depolarization evoked by cooling (Pertusa and Madrid, 2017). We hypothesized that pharmacological block of the K_V1 current *in vivo* would therefore unmask silent cold-sensing neurons. We imaged sensory neuron responses to cooling in Pirt-GCaMP3 mice at baseline and 30 minutes after intraplantar injection of the non-specific voltage-gated potassium channel blocker 4-aminopyridine (4-AP, 10 mM in 20 µl) (**Fig. 7A**). 4-AP treatment triggered *de novo* sensitivity to cooling in previously cold-insensitive large diameter neurons (**Fig. 7A-D**). Intriguingly, the effect of 4-AP was reduced by pre-treatment with oxaliplatin (**Fig. 7B-D**).

Treatment with the selective K_V1 antagonist α-dendrotoxin (100 µM) mimicked the effect of 4-AP (**Fig. 7B-D**), indicating block of K_V1 channels alone is sufficient to induce *de novo* cold sensitivity in silent cold-sensing neurons. k-dendrotoxin at 100 µM, a specific blocker of $K_V1.1$, largely recapitulated the effect of α-dendrotoxin on silent cold-sensing neurons (**Fig. 7B-D**). The $K_V1.2$ blocker Conotoxin kM-RIIIJ (100 µM) had only minor effects (**Fig. 7B-D**). 4-AP and α-dendrotoxin, but not k-dendrotoxin, increased the number of mechano-cold polymodal neurons (**Fig. 7E**). Interestingly, no potassium channel blocker modified the activity of the basally-active population of cold neurons (**Fig. 7F**). Overall, these data suggest that a functional reduction in K_V1 channels, primarily mediated through $K_V1.1$, could act as a molecular switch to trigger *de novo* cold sensitivity in silent cold-sensing neurons and therefore may also contribute to their unmasking during neuropathic pain (**Fig. 8**).

Discussion

Silent cold-sensing neurons become active during neuropathic pain

Here we have found using *in vivo* imaging that activation of normally silent, large-diameter silent cold-sensing neurons is a common mechanism of cold allodynia in three models of clinically important neuropathic pain states. The silent cold-sensing neurons identified here typically had functional and molecular characteristics consistent with peptidergic A-fibre nociceptors (Lawson *et al.*, 2019). Crucially we observed no changes in cold thresholds in the basally-active population of cold-sensing neurons. Thus, our findings suggest cold allodynia is a form of peripheral sensitization where a subpopulation of nociceptors gains an inappropriate sensitivity to the cold. This contrasts with tactile allodynia, which depends on peripheral drive from low-threshold mechanoreceptors expressing Piezo2 (Eijkelkamp *et al.*, 2013; Murthy *et al.*, 2018; Szczot *et al.*, 2018).

Electrophysiological recording of both rodent and human nerves exposed to oxaliplatin reveals myelinated A fibres fire more in the cold (Kagiava *et al.*, 2008; Sittl *et al.*, 2010, 2012). Blockade of large fibres abolishes cold allodynia in humans with non-freezing cold injury and oxaliplatin neuropathy (Forstenpointner *et al.*, 2018; Jørum and Opstad, 2019). Nerve injury and ciguatoxin likewise increase the fraction of cold-sensitive cutaneous sensory neurons *in vitro* (Vetter *et al.*, 2012; González *et al.*, 2017). There is a gradation – fewer silent cold-sensing neurons are recruited by nerve injury compared to oxaliplatin or ciguatoxin-2, and cold allodynia is correspondingly less prevalent in these patients (Yin *et al.*, 2015; MacDonald *et al.*, 2020). Nonetheless, because silent cold-sensing neurons are unmasked in all three neuropathic pain states tested here, our results do support a common underlying pathophysiology.

In the healthy state, a sparse and modality-specific subpopulation of small-diameter sensory neurons signals cooling (Emery *et al.*, 2016; Yarmolinsky *et al.*, 2016; Wang *et al.*, 2018). During neuropathy we find this ‘labelled line’ breaks down, with large neurons responding to both cold and noxious mechanical pinch, but rarely to heat, touch and punctate mechanical stimuli. The percentage of silent cold-sensing neurons sensitive to pinch is likely an under-estimate due to the differing receptive field areas of these two stimuli. Interestingly, inflammatory mediators also increase the number of polymodal neurons (Emery *et al.*, 2016). Enhanced polymodality is thus a general feature of sensitized pain states (Emery and Wood, 2019).

Molecular identity of silent cold-sensing neurons

Despite their large size, silent cold-sensing neurons did not express molecular markers for Aβ (*Calb1*) and Aδ (*Ntrk2*) low-threshold mechanoreceptors. This was surprising given that oxaliplatin preferentially modulates A fibre activity (Kagiava *et al.*, 2008; Sittl *et al.*, 2010, 2012; Forstenpointner *et al.*, 2018). However, our findings are consistent with the essential role of *Ntrk2*-positive neurons in tactile but not cold allodynia, indicating distinct modalities of allodynia are mechanistically different (Cobos *et al.*, 2018; Dhandapani *et al.*, 2018).

The majority of silent cold-sensing neurons expressed the nociceptor marker $Na_V1.8$ (Abrahamsen *et al.*, 2008). Although $Na_V1.8$ is not a selective marker of silent cold-sensing neurons, very few of the small diameter, basal cold-sensing cells express this sodium channel (Luiz *et al.*, 2019). Thus DTA-mediated ablation of $Na_V1.8$-positive neurons in healthy mice had no effect on the moderate cold assays used here to examine allodynia. But after oxaliplatin treatment, deletion of $Na_V1.8$-positive neurons including the newly unmasked cold sensors did result in diminished cold allodynia, mechanistically linking silent cold-sensing neurons with cold allodynia. Consistent with this, $Na_V1.8$-DTA mice were previously shown to have deficient cold allodynia elicited by ciguatoxin-1, while deletion of HCN2 channels specifically in $Na_V1.8$-positive neurons impairs cold allodynia in chronic constriction injury (Emery *et al.*, 2011; Vetter *et al.*, 2012).

We found that most silent cold-sensing neurons express CGRPα, but not Tmem45b, and are therefore likely peptidergic nociceptors. Large-diameter, NF200-expressing neurons that are CGRPα-positive, but Trpv1-negative, have been implicated in mechanical nociception, in tune with our finding that a subset of silent cold-sensing neurons responded to pinch (Scherrer *et al.*, 2009). Indeed, *in vivo* imaging of the trigeminal ganglion has shown that CGRPα-positive neurons are a mixture of small-diameter polymodal nociceptors and large-diameter mechanonociceptors that respond to noxious mechanical stimulation (Ghitani *et al.*, 2017). Another trigeminal imaging study revealed that, following burn injury of the oral cavity, previously ‘silent’ CGRPα-positive neurons became newly sensitive to cooling (Yarmolinsky *et al.*, 2016). Tellingly, optogenetic inhibition of CGRPα-positive neurons transiently and reversibly relieves cold allodynia after spared nerve injury (Cowie *et al.*, 2018).

Taken together, these results identify silent cold-sensing neurons as mainly peptidergic nociceptors that express *Scn10a* and *Calca* molecular markers. Extending our previous observations that $Na_V1.8$-positive sensory neurons signal prolonged and extreme cold, a further potential role for these nociceptors in mediating pathological responses to normal cooling is now apparent (Luiz *et al.*, 2019).

Ionic mechanisms of *de novo* cold sensitivity

We previously found that voltage-gated potassium channels $K_V1.1$ and $K_V1.2$ were enriched in basally cold-insensitive, $Na_V1.8$-positive neurons (Luiz *et al.*, 2019). Silent cold-sensing neurons therefore have high baseline expression of K_V1 channels which pass a voltage-dependent excitability brake current opposing cold-induced depolarization (Madrid *et al.*, 2009; González *et al.*, 2017). Blocking K_V1 voltage-gated potassium channels with 4-aminopyridine or α-dendrotoxin consequently induced *de novo* cold sensitivity in silent cold-sensing neurons, and this effect was partially recapitulated by inhibiting $K_V1.1$, but not $K_V1.2$. Although oxaliplatin and P-CTX-2 directly activate voltage-gated sodium channels, potentiating sodium channels does not drive *de novo* cold-sensitivity, indicating that ectopic cold activation is not a consequence of a general increase in excitability, but specifically linked to inhibiting K_V1 channels (Sittl *et al.*, 2012; Inserra *et al.*, 2017). Indeed, K_V1 channels are known to potently control action potential firing in response to sensory stimuli in both cold- and mechanically-sensitive nerve terminals (Madrid *et al.*, 2009; Hao *et al.*, 2013).

Does neuropathic pain lead to functional downregulation of K_V1 channels? 4-AP induces *de novo* cold sensitivity in sensory neurons from control, but not nerve injured, mice (González *et al.*, 2017). 4-AP evoked behavioural cold hypersensitivity is also suppressed in injured animals, indicating that nerve injury-induced cold allodynia operates via the same pathway as 4-AP to drive *de novo* cold sensitivity (González *et al.*, 2017). Corroborating this, we found that 4-AP unmasked fewer silent cold-sensing neurons in mice pre-treated with oxaliplatin. The mechanism of K_V1 channel of downregulation is unclear and is likely to be specific to each disease state. Quantitative PCR of samples from oxaliplatin-treated mice reveal that there is a decrease in $K_V1.1$ RNA, supporting transcriptional changes (Descoeur *et al.*, 2011). Numerous reports have also found a decrease in both $K_V1.1$ and $K_V1.2$ expression following nerve injury (Ishikawa *et al.*, 1999; Rasband *et al.*, 2001; Kim *et al.*, 2002; Park *et al.*, 2003; Yang *et al.*, 2004; Zhao *et al.*, 2013; Calvo *et al.*, 2016). On the other hand, *in vitro* studies support a direct antagonist effect of both oxaliplatin and ciguatoxin on voltage-gated potassium channels (Birinyi-Strachan *et al.*, 2005; Sittl *et al.*, 2010). However, it is important to note that a causal link between peripheral neuropathy and K_V1 channel activity was not investigated or explicitly demonstrated in our study.

Conclusions

Overall, we show that cold allodynia results from a set of normally silent cold-sensing neurons gaining *de novo* cold sensitivity in neuropathic pain. Cold allodynia is therefore a form of peripheral sensitization. Silent cold-sensing neurons were identified as putative A-fibre peptidergic nociceptors based on their large diameter, response to noxious mechanical stimulation, and expression of molecular markers $Na_V1.8$ and CGRPα. Block of K_V1 channels is sufficient to induce *de novo* cold sensitivity, pointing to downregulation of these channels during disease as a possible trigger of cold allodynia. By defining cells and molecules involved in cold allodynia, our findings will inform the development of better targeted therapeutics for neuropathic pain. The *in vivo* imaging data collected here provides a unique insight into the mechanisms underpinning cold allodynia, for the first time identifying silent cold-sensing neurons as critical drivers of cold-evoked neuropathic pain.

Acknowledgements

We thank Xinzhong Dong for Pirt-GCaMP3 mice, David Ginty and members of the Molecular Nociception Group for Cre-lines, Richard Lewis for the gift of ciguatoxin-2, and Aida Marcotti for help with cold pain behaviour tests. We thank James Cox and other members of the Molecular Nociception Group for help and advice.

Funding

This research was supported by the Wellcome Trust (200183/Z/15/Z), MRC, Wolfson Foundation and Versus Arthritis (20200).

Competing interests

The authors declare no conflict of interest.

Fig. 1. Silent cold-sensing neurons are activated by oxaliplatin.

(A) Behavioural testing of the effect of intraplantar oxaliplatin injection on different sensory modalities (cold, mechanical and heat). n=8 (5♂ & 3♀) for vehicle and n=9 for oxaliplatin (5♂ & 4♀). Mean values before and after treatment were compared using repeated measures 2-way ANOVA followed by post-hoc Sidak's test. Error bars denote 95% confidence interval.

(B) Example images (i.) and traces (ii.) of cold-responding neurons in vehicle- and oxaliplatin-treated animals expressing GCaMP3. Cell #1 is a small-diameter cold-sensing neuron in the vehicle condition, Cell #2 is a small-diameter basal cold-sensing neuron after oxaliplatin and Cell #3 is a large-diameter silent cold-sensing neuron unmasked by oxaliplatin that also responds to noxious mechanical stimuli

(C) (i.) Histograms of cross-sectional area of all neurons responding to any cold stimulus in vehicle (top, blue, n=82) and oxaliplatin (bottom, red, n=179) groups. The distribution of areas for vehicle was fit by non-linear regression (least squares Gaussian; Bin width is 80 μm^2 ; Mean=214.9 μm^2 , Std. Dev (σ)=77.29 μm^2). This model is plotted over the oxaliplatin data to aid comparison with the dashed line denoting three standard deviations from the mean. The different in the distribution of areas between groups was assessed by Kolmogorov-Smirnov test ($p<0.001$). (ii.) Bar plot of the percentage of responding neurons classed as silent cold-sensing neurons in vehicle and oxaliplatin groups. Proportions were compared using a χ^2 test, and error bars denote 95% confidence intervals.

(D) Relationship between the number of basal cold-sensing neurons and the drop in temperature can be fit by linear regression for both groups. For vehicle, $y = -2.883 * x + 105.2$, $r^2=0.9809$, n=87. For basal cold-sensing neurons afer oxaliplatin, $y = -3.443 * x + 105$, $r^2=0.9802$, n=39. The slopes are not significantly different ($p=0.12$).

(E) Quantification of the proportion of cold-sensing neurons responding to either heat (i.) or mechanical (ii.) stimuli in vehicle and oxaliplatin groups. The proportion of polymodal neurons was compared using χ^2 test, and error bars denote confidence intervals. Ice water: $n_{veh}=51$, $n_{oxa}=81$. Acetone: $n_{veh}=58$, $n_{oxa}=145$. (iii.) Cumulative probability plots showing mechano-cold neurons tend to have larger cross-sectional areas in the oxaliplatin group, compared using the Kolmogorov-Smirnov test. $n_{veh}=14$, $n_{oxa}=62$.

For this experiment, 383 neurons responding to any stimulus were recorded in 8 vehicle-treated mice (5♂ & 3♀) and 542 cells were recorded from 9 oxaliplatin-treated animals (5♂ & 4♀)

Fig. 2. Silent cold sensing neurons are activated after partial sciatic nerve ligation.

(A) Behavioural testing of the effect of partial sciatic nerve ligation (PNL) on different sensory modalities. n=3 (1♂ & 2♀) for sham and n=6 (3♂ & 3♀) for PNL. For Von Frey and Acetone test, means over time were compared using repeated measures 2-way ANOVA followed by post-hoc Sidak's test. Hot Plate latencies at 4 weeks were compared using unpaired t test. Error bars denote standard error of the mean.

(B) Example images (i.) and traces (ii.) of cold-responding neurons in sham- and PNL-operated animals expressing GCaMP3. Cell #1 is a small-diameter cold-sensing neuron in the sham condition, Cell #2 is a small-diameter basal cold-sensing neuron after PNL and Cell #3 is a large-diameter silent cold-sensing neuron unmasked by PNL.

(C) (i.) Histograms of cross-sectional area of all neurons responding to any cold stimulus in sham (top, blue, n=113) and PNL (bottom, red, n=109) groups. The distribution of areas for sham was fit by non-linear regression (least squares Gaussian; Bin width is 80 μm^2 ; Mean=222.7 μm^2 , Std. Dev. 60.9 μm^2). This model is plotted over the PNL data to aid comparison with the dashed line denoting three standard deviations from the mean. The different in the distribution of areas between groups was assessed by Kolmogorov-Smirnov test ($p<0.001$). (ii.) Bar plot of the percentage of responding neurons classed as silent cold-sensing neurons in sham and PNL groups. Proportions were compared using a χ^2 test, and error bars denote confidence intervals.

(D) Relationship between the number of basal cold-sensing neurons and the drop in temperature can be fit by linear regression for both groups. For sham, $y = -3.603 * x + 101.6$, $r^2=0.9979$, n=51. For PNL, $y = -3.875 * x + 107.8$, $r^2=0.9598$, n=40. The slopes are not significantly different ($p=0.66$).

(E) Quantification of the proportion of cold-sensing neurons responding to either heat (i.) or mechanical (ii.) stimuli in sham and PNL groups. The proportion of polymodal neurons was compared using χ^2 test, and error bars denote confidence intervals. Ice-water: n_{sham}=64, n_{PNL}=71. Acetone: n_{sham}=95, n_{PNL}=73. (iii.) Scatter plots showing mechano-cold neurons have both small and large cross-sectional areas in the PNL group. n_{sham}=3, n_{PNL}=19.

For this experiment, 373 neurons responding to any stimulus were recorded in 3 sham-operated mice (1♂ & 2♀) and 297 cells were recorded from 6 PNL-operated animals (3♂ & 3♀).

Fig. 3. Silent cold-sensing neurons are activated by ciguatoxin-2.

(A) Behavioural testing of the effect of intraplantar injection of 100 nM ciguatoxin-2 (P-CTX-2) on cold sensitivity n=6 for sham vehicle (3♂ & 3♀) and n=6 for P-CTX-2 (3♂ & 3♀). Means were compared by repeated measures 2-way ANOVA followed by post-hoc Sidak's test. Error bars denote 95% confidence interval.

(B) Example images and traces of a large-diameter neuron (Cell #1) that is basally cold-insensitive but begins to respond to cooling after treatment with P-CTX-2.

(C) (i.) Heatmap showing the effect of P-CTX-2 on the number of neurons responding to a cold ice-water stimulus. n=48 for vehicle, and n=196 for P-CTX-2. The bar corresponds to 15 s. (ii.) Summary of the change in the number of sensory neurons responding to each modality after treatment with P-CTX-2.

(D) Histograms of cross-sectional area of all neurons responding to any cold stimulus in the naïve state (left, blue, n=91) and after P-CTX-2 (right). For P-CTX-2, blue denotes basally-responsive neurons that maintained their response to cold (n=70) and red denotes the silent cold-sensing neurons that were unmasked after treatment (n=136). The distribution of areas in the naïve state was fit by non-linear regression (least squares Gaussian; Bin width is 80 μm^2; Mean=212.4 μm^2, Std. Dev. 73.33 μm^2). This model is plotted over the P-CTX-2 data to aid comparison with the dashed line denoting three standard deviations from the mean. The different in the distribution of areas between groups was assessed by Kolmogorov-Smirnov test (p<0.001).

(E) (i.) Box plot of the change in activation threshold of basally cold-sensitive neurons before and after treatment with vehicle (n=35) or P-CTX (n=8). ii.) Box plot of the thermal activation threshold of all silent cold-sensing neurons unmasked by P-CTX-2 (n=43) compared to all cold-sensing neurons recorded from naïve mice (n=62). Medians were compared by Mann-Whitney test.

(F) Quantification of the proportion of neurons responding ice-water that were also sensitive to either mechanical (i.) or heat (ii.) before and after treatment. Vehicle: n_{pre}=36, n_{post}=43. P-CTX-2: n_{pre}=69, n_{post}=174. (iii.) Comparison of the proportion of silent cold-sensing neurons that were responsive to other modalities before and after the induction of cold-sensitivity by P-CTX-2. n=127. The proportion of polymodal neurons was compared using χ^2 test, and error bars denote 95% confidence intervals.

For this experiment, 615 neurons responding to any stimulus either before or after treatment were recorded in 10 P-CTX-2-injected mice (4♂ & 6♀) and 193 cells were recorded from 3 vehicle-injected animals (2♂ & 1♀).

Fig. 4. Silent cold-sensing neurons express peptidergic nociceptor molecular markers $Na_V1.8$ and CGRPα.

(A) Cartoon (left) of breeding strategy used to generate GCaMP3 reporter mice for each subset of interest. Bar plot (right) showing overlap of reporter expression for each marker with functionally-defined cold-sensing neurons.

TrkB-CreERT2 (*Ntrk2*): n_{veh}=14 from 2 mice (1♂ & 1♀)), n_{oxa}=112 from 3 mice (2♂ & 1♀). Calb1-Cre (*Calb1*): n_{veh}=7 from 1 mouse (1♂), n_{oxa}=15 from 2 mice (2♀). Trpv1-Cre (*Trpv1*): n_{veh}=4 from 1 mouse (1♂), n_{oxa}=87 from 2 mice (1♂ & 1♀). $Na_V1.8$-Cre (*Scn10a*): n_{veh}=14 from 4 mice (2♂ & 2♀), n_{oxa}=108 from 6 mice (4♂ & 2♀). Tmem45b-Cre (*Tmem45b*): n_{veh}=40 from 1 mouse (1♂), n_{oxa}=36 from 3 mice (2♂ & 1♀). CGRPα-CreERT2 (*Calca*): n_{veh}=45 from 3 mice (1♂ & 2♀), n_{oxa}=122 from 2 mice (1♂ & 1♀).

(B) Example images (left) and histograms (right) showing overlap of $Na_V1.8$-Cre-dependent tdTomato expression with cold-sensing neurons of different sizes in vehicle- and oxaliplatin-treated mice. Same data as in (A).

(C) Histogram (left) and bar plot (right) showing overlap of $\text{Na}_\text{V}1.8$-Cre-dependent tdTomato expression with different types of cold-sensing neurons in PNL-operated mice. n=57 cells from 2 mice (1♂ & 1♀).

(D) Histograms (left) and bar plot (right) showing overlap of $\text{Na}_\text{V}1.8$-Cre-dependent tdTomato expression with basally-active and silent cold-sensing neurons in mice treated with P-CTX-2. n=56 cells from 4 mice (1♂ & 3♀).

(E) Example images (left) and histograms (right) showing overlap of CGRPα-CreERT2-dependent tdTomato expression with cold-sensing neurons of different sizes in vehicle- and oxaliplatin-treated mice. Same data as in (A).

(F) Histogram (left) and bar plot (right) showing overlap of CGRPα-CreERT2-dependent tdTomato expression with different types of cold-sensing neurons in PNL-operated mice. n=16 cells from 1 mouse (1♂).

(G) Histograms (left) and bar plot (right) showing overlap of CGRPα-CreERT2-dependent tdTomato expression with basally-active and silent cold-sensing neurons in mice treated with P-CTX-2. n=56 cells from 2 mice (1♂ & 1♀).

Error bars denote 95% confidence intervals. As these data were obtained as part of an exploratory screen, no statistical hypothesis testing was performed.

Fig. 5. Diphtheria toxin-mediated ablation of $\text{Na}_\text{V}1.8$-positive nociceptors decreases oxaliplatin-induced cold allodynia.

(A) Cartoon of diphtheria toxin-mediated ablation of $\text{Na}_\text{V}1.8$-positive neurons.

(B) (i.) Histogram of cross-sectional areas of all cold-sensing neurons imaged in $\text{Na}_\text{V}1.8$-Cre DTA mice treated with oxaliplatin. (ii.) Cumulative probability plot of cell areas in oxaliplatin-treated $\text{Na}_\text{V}1.8$-Cre (blue) and $\text{Na}_\text{V}1.8$-Cre DTA (red) mice, compared by Kolmogorov-Smirnov test. The distribution of cell areas in vehicle-treated $\text{Na}_\text{V}1.8$-Cre mice is shown for comparison. n=108 cells from 6 oxaliplatin-treated $\text{Na}_\text{V}1.8$-Cre mice (4♂ & 2♀), n=46 cells from 2 oxaliplatin-treated $\text{Na}_\text{V}1.8$-Cre DTA mice (1♂ & 1♀), and n=14 cells from 4 vehicle-treated $\text{Na}_\text{V}1.8$-Cre mice (2♂ & 2♀).

(C) Quantification of the number of nociceptive behaviours in 5 minutes on the 5°C Cold Plate in 10 control and 8 $\text{Na}_\text{V}1.8$-Cre DTA mice treated with oxaliplatin.

Fig. 6. Voltage-gated sodium channel $\text{Na}_\text{V}1.6$ is required for excitability, but is not sufficient for cold sensitivity, of silent cold-sensing neurons.

(A) (i.) Histogram of cross-sectional areas of all cold-sensing neurons imaged in homozygous $\text{Na}_\text{V}1.8$-Cre tdTomato mice with oxaliplatin. (ii.) Cumulative probability plot of cell areas in oxaliplatin-treated heterozygous and homozygous $\text{Na}_\text{V}1.8$-Cre mice, compared by Kolmogorov-Smirnov test. (iii.) Bar plot showing the proportion of silent cold-sensing neurons expressing tdTomato in heterozygous and homozygous $\text{Na}_\text{V}1.8$-Cre mice, compared using χ^2 test. n=66 cells from 6 heterozygous (2♂ & 1♀) and n=42 cells from 3 homozygous (1♂ & 2♀) $\text{Na}_\text{V}1.8$-Cre mice.

(B) Cumulative probability plot of cell areas in oxaliplatin-treated WT and $\text{Na}_\text{V}1.7$ KO mice, compared by Kolmogorov-Smirnov test. n=51 cells from 5 WT (1♂ & 4♀) and n=18 cells from 2 $\text{Na}_\text{V}1.7$ KO mice (2♀).

(C) Heat maps (i.) and quantification (ii.) showing the effect of intraplantar injection of different sodium channel blockers on the number of basal and silent cold-sensing neurons in mice pre-treated with oxaliplatin. (iii.) Line plot showing the effect of blockers on median peak response, compared using Kruskall-Wallis test followed by Dunn's multiple comparisons test. n=35 cells from 3 mice for saline (1♂ & 2♀), n=58 cells from 4 mice for TTX (3♂ & 1♀), n=36 cells from 2 mice for 4,9-anhydrous-TTX (2♀).

(D) (i.) Heat map showing the effect of sodium channel activation by intraplantar veratridine injection on the activity of cold-sensing neurons. (ii.) Box plot showing the size of cold-sensing cells is unaffected by veratridine, compared by Mann-Whitney test. (iii.) Bar plot showing veratridine reduces the number of cold-sensing neurons from 39 to 31. (iv.) Line plot showing veratridine reduces the response magnitude of cold-sensing cells, compared by Wilcoxon matched-pairs signed rank test. n=53 cells from 3 mice (3♂).

Fig. 7. Blocking $K_V1.1$ voltage-gated potassium channels is sufficient to induce de novo cold sensitivity in silent cold-sensing neurons.

(A) Examples images and traces showing that peripheral blockade of voltage-gated potassium channels induces novel cold-sensitivity in normally cold-insensitive sensory neurons (Cell #1).

(B) Heat maps showing the effect of intraplantar injection of different potassium channel blockers on the peripheral representation of cold. The bar denotes 15 s.

(C) Quantification showing the change in the number of cold-sensing neurons after treatment with different potassium channel blockers.

(D) Violin plots showing the cross-sectional area of basal cold-sensing neurons in the naïve state (blue) and of silent cold-sensing neurons unmasked by potassium channel block (red). Medians were compared using Kruskall-Wallis test followed by Dunn's multiple comparison test.

(E) Bar plot of the percentage of polymodal cold-sensing neurons that also respond to noxious mechanical stimuli before (blue) and after (red) treatment with potassium channel blockers. Proportions were compared using a χ^2 test. Error bars denote 95% confidence intervals.

(F) No change in the median response magnitude of neurons that responded to cold both before (blue) and after (red) treatment with potassium channel blockers, as determined by Kruskall-Wallis test followed by Dunn's multiple comparison test.

n=42 from 3 saline-treated mice (1♂ & 2♀), n=57 from 6 4-AP-treated mice (5♂ & 1♀), n=95 from 3 4-AP-treated mice pre-injected with oxaliplatin (2♂ & 1♀), n=101 from 4 α-dendrotoxin-treated mice (2♂ & 2♀), n=48 from 3 k-dendrotoxin-treated mice (1♂ & 2♀), and n=14 from 3 RIIIJ-treated mice (3♀).

Fig. 8. Proposed model of silent cold-sensing neuron activation during neuropathy to cause cold allodynia

In healthy mice, only small neurons respond to cold. The large-diameter silent cold-sensing neurons have high K_V1 activity, thus cold-induced terminal depolarization does not trigger action potential firing and there is no subsequent GCaMP signal at the level of the dorsal root ganglion.

In neuropathic animals, we hypothesize that a functional reduction in K_V1 activity means that silent cold-sensing neurons are now sensitive to cold, increasing nociceptive input to the brain in response to cooling. Thus both small and large neurons now show GCaMP signals to cold stimuli.

List of references

Abrahamsen B, Zhao J, Asante CO, Cendan CM, Marsh S, Martinez-Barbera JP, et al. The cell and molecular basis of mechanical, cold, and inflammatory pain. Science 2008; 321: 702–5.

Akopian AN, Souslova V, England S, Okuse K, Ogata N, Ure J, et al. The tetrodotoxin-resistant sodium channel SNS has a specialized function in pain pathways. Nat Neurosci 1999; 2: 541–8.

Alloui A, Zimmermann K, Mamet J, Duprat F, Noël J, Chemin J, et al. TREK-1, a K+ channel involved in polymodal pain perception. EMBO J 2006; 25: 2368–76.

Bautista DM, Siemens J, Glazer JM, Tsuruda PR, Basbaum AI, Stucky CL, et al. The menthol receptor TRPM8 is the principal detector of environmental cold. Nature 2007; 448: 204–8.

Birinyi-Strachan LC, Gunning SJ, Lewis RJ, Nicholson GM. Block of voltage-gated potassium channels by Pacific ciguatoxin-1 contributes to increased neuronal excitability in rat sensory neurons. Toxicol Appl Pharmacol 2005; 204: 175–86.

von Buchholtz LJ, Ghitani N, Lam RM, Licholai JA, Chesler AT, Ryba NJP. Decoding Cellular Mechanisms for Mechanosensory Discrimination. Neuron 2020; 109: 1–14.

Calvo M, Richards N, Schmid AB, Barroso A, Zhu L, Ivulic D, et al. Altered potassium channel distribution and composition in myelinated axons suppresses hyperexcitability following injury. Elife 2016; 5

Cobos EJ, Nickerson CA, Gao F, Chandran V, Bravo-Caparrós I, González-Cano R, et al. Mechanistic Differences in Neuropathic Pain Modalities Revealed by Correlating Behavior with Global Expression Profiling. Cell Rep 2018; 22: 1301–12.

Colburn RW, Lubin M Lou, Stone DJ, Wang Y, Lawrence D, D’Andrea MR, et al. Attenuated cold sensitivity in TRPM8 null mice. Neuron 2007; 54: 379–86.

Cowie AM, Moehring F, O’Hara C, Stucky CL. Optogenetic Inhibition of CGRPα Sensory Neurons Reveals Their Distinct Roles in Neuropathic and Incisional Pain. J Neurosci 2018; 38: 5807–25.

Descoeur J, Pereira V, Pizzoccaro A, Francois A, Ling B, Maffre V, et al. Oxaliplatin-induced cold hypersensitivity is due to remodelling of ion channel expression in nociceptors. EMBO Mol Med 2011; 3: 266–78.

Deuis JR, Zimmermann K, Romanovsky AA, Possani LD, Cabot PJ, Lewis RJ, et al. An animal model of oxaliplatin-induced cold allodynia reveals a crucial role for Nav1.6 in peripheral pain pathways. Pain 2013; 154: 1749–57.

Dhaka A, Murray AN, Mathur J, Earley TJ, Petrus MJ, Patapoutian A. TRPM8 is required for cold sensation in mice. Neuron 2007; 54: 371–8.

Dhandapani R, Arokiaraj CM, Taberner FJ, Pacifico P, Raja S, Nocchi L, et al. Control of mechanical pain hypersensitivity in mice through ligand-targeted photoablation of TrkB-positive sensory neurons. Nat Commun 2018; 9: 1640.

Eijkelkamp N, Linley JE, Torres JM, Bee L, Dickenson AH, Gringhuis M, et al. A role for Piezo2 in EPAC1-dependent mechanical allodynia. Nat Commun 2013; 4

Emery EC, Luiz AP, Sikandar S, Magnúsdóttir R, Dong X, Wood JN. In vivo characterization of distinct modality-specific subsets of somatosensory neurons using GCaMP. Sci Adv 2016; 2: e1600990.

Emery EC, Wood JN. Somatosensation a la mode: plasticity and polymodality in sensory neurons. Curr Opin Physiol 2019; 11: 29–34.

Emery EC, Young GT, Berrocoso EM, Chen L, McNaughton PA. HCN2 ion channels play a central role in inflammatory and neuropathic pain. Science 2011; 333: 1462–6.

Forstenpointner J, Oberlojer VC, Naleschinski D, Höper J, Helfert SM, Binder A, et al. A-Fibers Mediate Cold Hyperalgesia in Patients with Oxaliplatin-Induced Neuropathy. Pain Pract 2018; 18: 758–67.

Ghitani N, Barik A, Szczot M, Thompson JH, Li C, Le Pichon CE, et al. Specialized Mechanosensory Nociceptors Mediating Rapid Responses to Hair Pull. Neuron 2017; 95: 944-954.e4.

González A, Ugarte G, Restrepo C, Herrera G, Piña R, Gómez-Sánchez JA, et al. Role of the Excitability Brake Potassium Current I_{KD} in Cold Allodynia Induced by Chronic Peripheral Nerve Injury. J Neurosci 2017; 37: 3109–26.

Hao J, Padilla F, Dandonneau M, Lavebratt C, Lesage F, Noël J, et al. Kv1.1 Channels Act as Mechanical Brake in the Senses of Touch and Pain. Neuron 2013; 77: 899–914.

Inserra MC, Israel MR, Caldwell A, Castro J, Deuis JR, Harrington AM, et al. Multiple sodium channel isoforms mediate the pathological effects of Pacific ciguatoxin-1. Sci Rep 2017; 7: 42810.

Ishikawa K, Tanaka M, Black JA, Waxman SG. Changes in expression of voltage-gated potassium channels in dorsal root ganglion neurons following axotomy. Muscle and Nerve 1999; 22: 502–7.

Jensen TS, Finnerup NB. Allodynia and hyperalgesia in neuropathic pain: clinical manifestations and mechanisms. Lancet Neurol 2014; 13: 924–35.

Jørum E, Opstad P-K. A 4-year follow-up of non-freezing cold injury with cold allodynia and neuropathy in 26 naval soldiers [Internet]. Scand J Pain 2019; 0[cited 2019 May 22] Available from: http://www.ncbi.nlm.nih.gov/pubmed/30939119

Kagiava A, Tsingotjidou A, Emmanouilides C, Theophilidis G. The effects of oxaliplatin, an anticancer drug, on potassium channels of the peripheral myelinated nerve fibres of the adult rat. Neurotoxicology 2008; 29: 1100–6.

Kim DS, Choi JO, Rim HD, Cho HJ. Downregulation of voltage-gated potassium channel alpha gene expression in dorsal root ganglia following chronic constriction injury of the rat sciatic nerve. Brain Res Mol Brain Res 2002; 105: 146–52.

Knowlton WM, Palkar R, Lippoldt EK, McCoy DD, Baluch F, Chen J, et al. A sensory-labeled line for cold: TRPM8-expressing sensory neurons define the cellular basis for cold, cold pain, and cooling-mediated analgesia. J Neurosci 2013; 33: 2837–48.

Lawson SN, Fang X, Djouhri L. Nociceptor subtypes and their incidence in rat lumbar dorsal root ganglia (DRGs): focussing on C-polymodal nociceptors, Aβ-nociceptors, moderate pressure receptors and their receptive field depths. Curr Opin Physiol 2019; 11: 125–46.

Lolignier S, Bonnet C, Gaudioso C, Noël J, Ruel J, Amsalem M, et al. The Nav1.9 Channel Is a Key Determinant of Cold Pain Sensation and Cold Allodynia. Cell Rep 2015; 11: 1067–78.

Luiz AP, MacDonald DI, Santana-Varela S, Millet Q, Sikandar S, Wood JN, et al. Cold sensing by NaV1.8-positive and NaV1.8-negative sensory neurons. Proc Natl Acad Sci U S A 2019; 116: 3811–6.

MacDonald DI, Wood JN, Emery EC. Molecular mechanisms of cold pain. Neurobiol Pain 2020; 7: 100044.

Madrid R, de la Pena E, Donovan-Rodriguez T, Belmonte C, Viana F. Variable Threshold of Trigeminal Cold-Thermosensitive Neurons Is Determined by a Balance between TRPM8 and Kv1 Potassium Channels. J Neurosci 2009; 29: 3120–31.

Mckemy DD. Therapeutic potential of Trpm8 modulators. Open Drug Discov J 2010; 2: 81–8.

Minett MS, Nassar MA, Clark AK, Passmore G, Dickenson AH, Wang F, et al. Distinct Nav1.7-dependent pain sensations require different sets of sensory and sympathetic neurons. Nat Commun 2012; 3: 791.

Morenilla-Palao C, Luis E, Fernández-Peña C, Quintero E, Weaver JL, Bayliss DA, et al. Ion Channel Profile of TRPM8 Cold Receptors Reveals a Role of TASK-3 Potassium Channels in Thermosensation. Cell Rep 2014; 8: 1571–82.

Murthy SE, Loud MC, Daou I, Marshall KL, Schwaller F, Kühnemund J, et al. The mechanosensitive ion channel Piezo2 mediates sensitivity to mechanical pain in mice. Sci Transl Med 2018; 10: eaat9897.

Nassini R, Gees M, Harrison S, De Siena G, Materazzi S, Moretto N, et al. Oxaliplatin elicits mechanical and cold allodynia in rodents via TRPA1 receptor stimulation. PAIN® 2011; 152: 1621–31.

Noël J, Zimmermann K, Busserolles J, Deval E, Alloui A, Diochot S, et al. The mechano-activated K+ channels TRAAK and TREK-1 control both warm and cold perception. EMBO J 2009; 28: 1308–18.

Park SY, Choi JY, Kim RU, Lee YS, Cho HJ, Kim DS. Downregulation of voltage-gated potassium channel α gene expression by axotomy and neurotrophins in rat dorsal root ganglia. Mol Cells 2003; 16: 256–9.

Pereira V, Busserolles J, Christin M, Devilliers M, Poupon L, Legha W, et al. Role of the TREK2 potassium channel in cold and warm thermosensation and in pain perception. PAIN® 2014; 155: 2534–44.

Pertusa M, Madrid R. The I_{KD} current in cold detection and pathological cold pain. Temperature

2017; 4: 346–9.

Pogorzala LA, Mishra SK, Hoon MA. The cellular code for mammalian thermosensation. J Neurosci 2013; 33: 5533–41.

Rasband MN, Park EW, Vanderah TW, Lai J, Porreca F, Trimmer JS. Distinct potassium channels on pain-sensing neurons. Proc Natl Acad Sci U S A 2001; 98: 13373–8.

Scherrer G, Imamachi N, Cao YQ, Contet C, Mennicken F, O'Donnell D, et al. Dissociation of the Opioid Receptor Mechanisms that Control Mechanical and Heat Pain. Cell 2009; 137: 1148–59.

Seltzer Z, Dubner R, Shir Y. A novel behavioral model of neuropathic pain disorders produced in rats by partial sciatic nerve injury. Pain 1990; 43: 205–18.

Sittl R, Carr RW, Fleckenstein J, Grafe P. Enhancement of axonal potassium conductance reduces nerve hyperexcitability in an in vitro model of oxaliplatin-induced acute neuropathy. Neurotoxicology 2010; 31: 694–700.

Sittl R, Lampert A, Huth T, Schuy ET, Link AS, Fleckenstein J, et al. Anticancer drug oxaliplatin induces acute cooling-aggravated neuropathy via sodium channel subtype Na(V)1.6-resurgent and persistent current. Proc Natl Acad Sci U S A 2012; 109: 6704–9.

Szczot M, Liljencrantz J, Ghitani N, Barik A, Lam R, Thompson JH, et al. PIEZO2 mediates injury-induced tactile pain in mice and humans. Sci Transl Med 2018; 10: eaat9892.

Usoskin D, Furlan A, Islam S, Abdo H, Lönnerberg P, Lou D, et al. Unbiased classification of sensory neuron types by large-scale single-cell RNA sequencing [Internet]. Nat Publ Gr 2014; 18[cited 2019 Jan 28] Available from: http://linnarssonlab.org/drg/

Vetter I, Touska F, Hess A, Hinsbey R, Sattler S, Lampert A, et al. Ciguatoxins activate specific cold pain pathways to elicit burning pain from cooling. EMBO J 2012; 31: 3795–808.

Viana F, Voets T. Heat Pain and Cold Pain [Internet]. In: The Oxford Handbook of the Neurobiology of Pain. Oxford University Press; 2019[cited 2019 May 23] Available from: http://oxfordhandbooks.com/view/10.1093/oxfordhb/9780190860509.001.0001/oxfordhb-9780190860509-e-13

Wang F, Bélanger E, Côté SL, Desrosiers P, Prescott SA, Côté DC, et al. Sensory Afferents Use Different Coding Strategies for Heat and Cold. Cell Rep 2018; 23: 2001–13.

Yang EK, Takimoto K, Hayashi Y, De Groat WC, Yoshimura N. Altered expression of potassium channel subunit mRNA and α-dendrotoxin sensitivity of potassium currents in rat dorsal root ganglion neurons after axotomy. Neuroscience 2004; 123: 867–74.

Yarmolinsky DA, Peng Y, Pogorzala LA, Rutlin M, Hoon MA, Zuker CS. Coding and Plasticity in the Mammalian Thermosensory System. Neuron 2016; 92: 1079–92.

Yin K, Zimmermann K, Vetter I, Lewis RJ. Therapeutic opportunities for targeting cold pain pathways. Biochem Pharmacol 2015; 93: 125–40.

Zeisel A, Hochgerner H, Lönnerberg P, Johnsson A, Memic F, van der Zwan J, et al. Molecular

Architecture of the Mouse Nervous System. Cell 2018; 174: 999-1014.e22.

Zhao X, Tang Z, Zhang H, Atianjoh FE, Zhao J-Y, Liang L, et al. A long noncoding RNA contributes to neuropathic pain by silencing Kcna2 in primary afferent neurons. Nat Neurosci 2013; 16: 1024–31.

Zimmermann K, Leffler A, Babes A, Cendan CM, Carr RW, Kobayashi J, et al. Sensory neuron sodium channel Nav1.8 is essential for pain at low temperatures. Nature 2007; 447: 855–8.

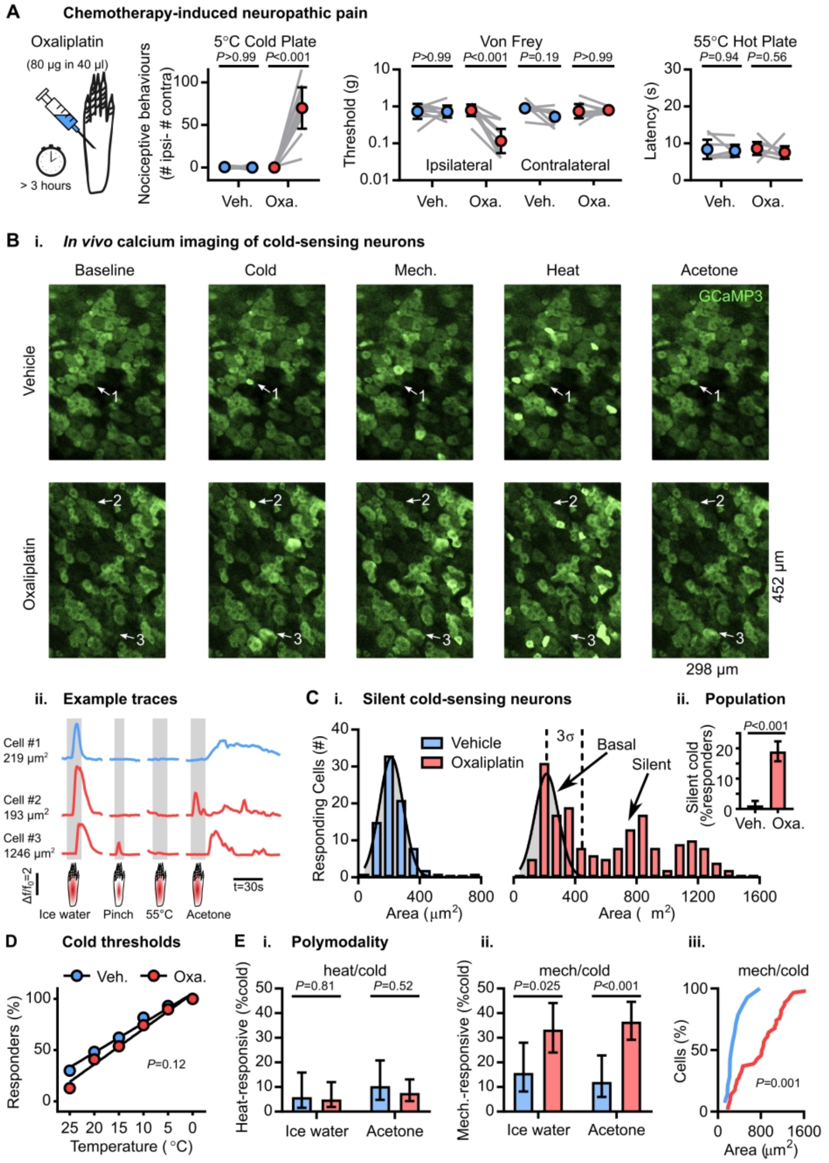
A Chemotherapy-induced neuropathic pain
Oxaliplatin
(80 µg in 40 µl)
> 3 hours
5°C Cold Plate
P>0.99
P<0.001
Nociceptive behaviours (# ipsi- # contra)
100
50
0
Veh.
Oxa.
Von Frey
P>0.99
P<0.001
P=0.19
P>0.99
Threshold (g)
10
1
0.1
0.01
Ipsilateral
Contralateral
Veh.
Oxa.
Veh.
Oxa.
55°C Hot Plate
P=0.94
P=0.56
Latency (s)
30
20
10
0
Veh.
Oxa.
B i. In vivo calcium imaging of cold-sensing neurons
Baseline
Cold
Mech.
Heat
Acetone
GCaMP3
Vehicle
Oxaliplatin
1
2
3
452 µm
298 µm
ii. Example traces
Cell #1 219 µm²
Cell #2 193 µm²
Cell #3 1246 µm²
Δf/f₀=2
t=30s
Ice water
Pinch
55°C
Acetone
C i. Silent cold-sensing neurons
Vehicle
Oxaliplatin
Responding Cells (#)
40
30
20
10
0
0
400
800
Area (µm²)
3σ
Basal
Silent
0
400
800
1200
1600
Area (µm²)
ii. Population
P<0.001
Silent cold (%responders)
20
10
0
Veh.
Oxa.
D Cold thresholds
Veh.
Oxa.
Responders (%)
100
50
0
25
20
15
10
5
0
Temperature (°C)
P=0.12
E i. Polymodality
heat/cold
P=0.81
P=0.52
Heat-responsive (%cold)
50
40
30
20
10
0
Ice water
Acetone
ii.
mech/cold
P=0.025
P<0.001
Mech.-responsive (%cold)
50
40
30
20
10
0
Ice water
Acetone
iii.
mech/cold
Cells (%)
100
50
0
P=0.001
0
800
1600
Area (µm²)

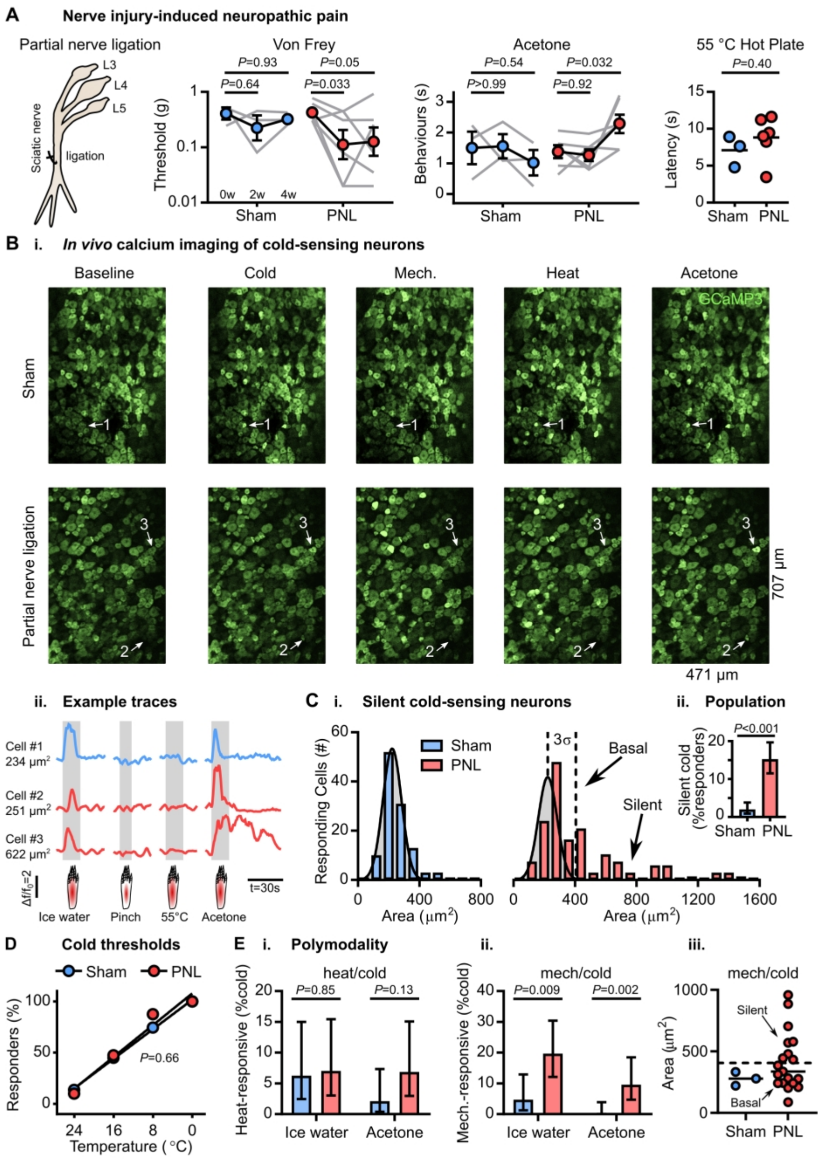
A
Nerve injury-induced neuropathic pain
Partial nerve ligation
L3
L4
L5
Sciatic nerve
ligation
Von Frey
P=0.93
P=0.05
P=0.64
P=0.033
Threshold (g)
1
0.1
0.01
0w
2w
4w
Sham
PNL
Acetone
P=0.54
P=0.032
P>0.99
P=0.92
Behaviours (s)
3
2
1
0
Sham
PNL
55 °C Hot Plate
P=0.40
Latency (s)
15
10
5
0
Sham
PNL
B i. In vivo calcium imaging of cold-sensing neurons
Baseline
Cold
Mech.
Heat
Acetone
GCaMP3
Sham
1
Partial nerve ligation
3
2
707 µm
471 µm
ii. Example traces
Cell #1 234 µm²
Cell #2 251 µm²
Cell #3 622 µm²
Δf/f₀=2
t=30s
Ice water
Pinch
55°C
Acetone
C i. Silent cold-sensing neurons
Sham
PNL
Responding Cells (#)
60
40
20
0
0
400
800
Area (µm²)
3σ
Basal
Silent
0
400
800
1200
1600
Area (µm²)
ii. Population
P<0.001
Silent cold (%responders)
20
10
0
Sham
PNL
D
Cold thresholds
Sham
PNL
Responders (%)
100
50
0
P=0.66
24
16
8
0
Temperature (°C)
E i. Polymodality
heat/cold
P=0.85
P=0.13
Heat-responsive (%cold)
20
15
10
5
0
Ice water
Acetone
ii.
mech/cold
P=0.009
P=0.002
Mech.-responsive (%cold)
40
30
20
10
0
Ice water
Acetone
iii.
mech/cold
Area (µm²)
1000
500
0
Silent
Basal
Sham
PNL

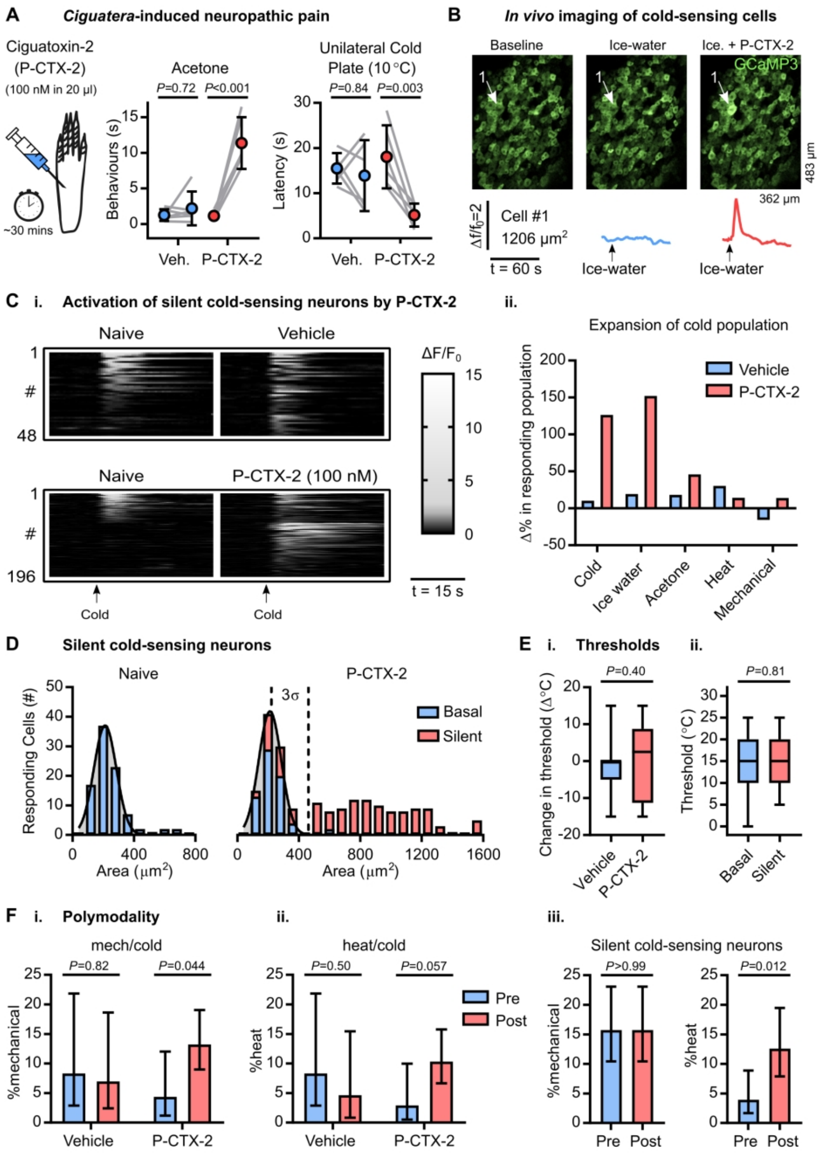
A
Ciguatera-induced neuropathic pain
Ciguatoxin-2
(P-CTX-2)
(100 nM in 20 µl)
~30 mins
Acetone
P=0.72
P<0.001
Behaviours (s)
15
10
5
0
Veh.
P-CTX-2
Unilateral Cold
Plate (10 °C)
P=0.84
P=0.003
Latency (s)
30
20
10
0
Veh.
P-CTX-2
B
In vivo imaging of cold-sensing cells
Baseline
Ice-water
Ice. + P-CTX-2
GCaMP3
1
483 µm
362 µm
Δf/f0=2
Cell #1
1206 µm²
t = 60 s
Ice-water
Ice-water
C i.
Activation of silent cold-sensing neurons by P-CTX-2
Naive
Vehicle
1
#
48
Naive
P-CTX-2 (100 nM)
1
#
196
Cold
Cold
ΔF/F0
15
10
5
0
t = 15 s
ii.
Expansion of cold population
Δ% in responding population
200
150
100
50
0
-50
Vehicle
P-CTX-2
Cold
Ice water
Acetone
Heat
Mechanical
D
Silent cold-sensing neurons
Naive
P-CTX-2
3σ
Responding Cells (#)
50
40
30
20
10
0
0
400
800
Area (µm²)
0
400
800
1200
1600
Area (µm²)
Basal
Silent
E i.
Thresholds
P=0.40
Change in threshold (Δ°C)
20
10
0
-10
-20
Vehicle
P-CTX-2
ii.
P=0.81
Threshold (°C)
30
25
20
15
10
5
0
Basal
Silent
F i.
Polymodality
mech/cold
P=0.82
P=0.044
%mechanical
25
20
15
10
5
0
Vehicle
P-CTX-2
ii.
heat/cold
P=0.50
P=0.057
%heat
25
20
15
10
5
0
Vehicle
P-CTX-2
Pre
Post
iii.
Silent cold-sensing neurons
P>0.99
P=0.012
%mechanical
%heat
25
20
15
10
5
0
Pre
Post
Pre
Post

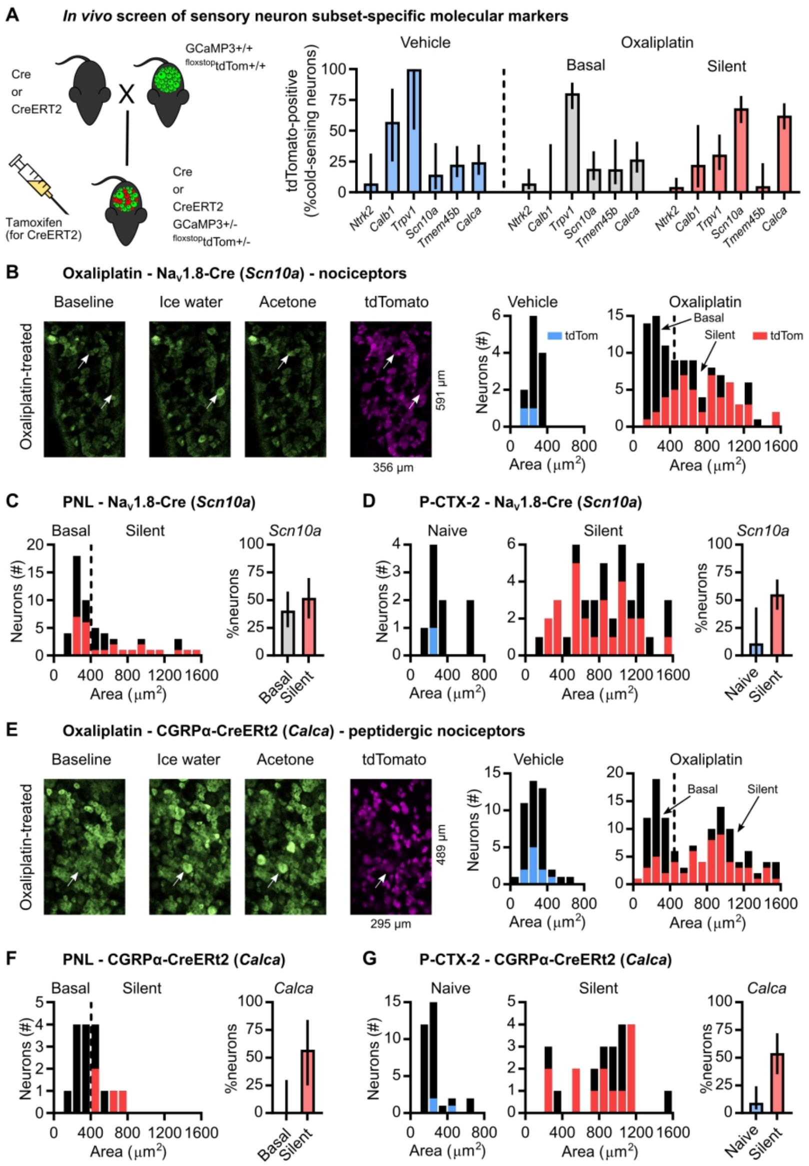
A
In vivo screen of sensory neuron subset-specific molecular markers
Cre or CreERT2
X
GCaMP3+/+ floxstoptdTom+/+
Tamoxifen (for CreERT2)
Cre or CreERT2 GCaMP3+/- floxstoptdTom+/-
tdTomato-positive (%cold-sensing neurons)
Vehicle
Oxaliplatin
Basal
Silent
Ntrk2
Calb1
Trpv1
Scn10a
Tmem45b
Calca
B
Oxaliplatin - Nav1.8-Cre (Scn10a) - nociceptors
Baseline
Ice water
Acetone
tdTomato
Oxaliplatin-treated
591 µm
356 µm
Vehicle
tdTom
Oxaliplatin
Basal
Silent
tdTom
Neurons (#)
Area (µm2)
C
PNL - Nav1.8-Cre (Scn10a)
Basal
Silent
Scn10a
%neurons
D
P-CTX-2 - Nav1.8-Cre (Scn10a)
Naive
Silent
Scn10a
E
Oxaliplatin - CGRPα-CreERt2 (Calca) - peptidergic nociceptors
Baseline
Ice water
Acetone
tdTomato
Oxaliplatin-treated
489 µm
295 µm
Vehicle
Oxaliplatin
Basal
Silent
F
PNL - CGRPα-CreERt2 (Calca)
Basal
Silent
Calca
G
P-CTX-2 - CGRPα-CreERt2 (Calca)
Naive
Silent
Calca

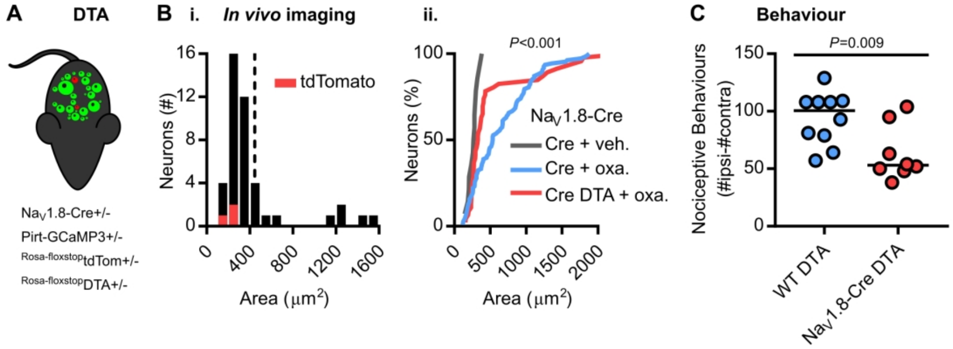
A
DTA
$Na_V1.8$-Cre+/-
Pirt-GCaMP3+/-
$^{Rosa-floxstop}$tdTom+/-
$^{Rosa-floxstop}$DTA+/-
B
i.
In vivo imaging
tdTomato
Neurons (#)
16
12
8
4
0
0
400
800
1200
1600
Area (μm^2)
ii.
P<0.001
Neurons (%)
100
50
0
0
500
1000
1500
2000
Area (μm^2)
$Na_V1.8$-Cre
Cre + veh.
Cre + oxa.
Cre DTA + oxa.
C
Behaviour
P=0.009
Nociceptive Behaviours (#ipsi-#contra)
150
100
50
0
WT DTA
$Na_V1.8$-Cre DTA

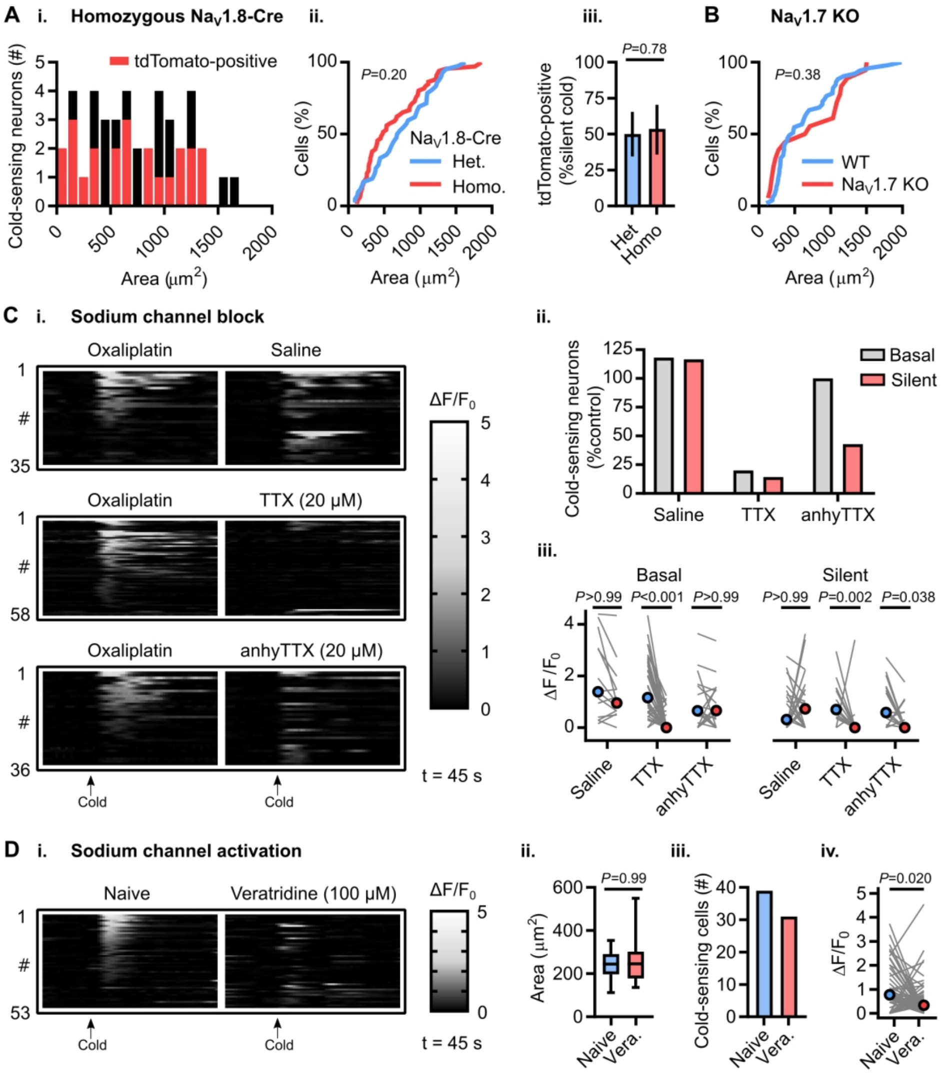

A i. Homozygous Na_V1.8-Cre
tdTomato-positive
Cold-sensing neurons (#)
5
4
3
2
1
0
0
500
1000
1500
2000
Area (μm^2)
ii.
P=0.20
Cells (%)
100
50
0
Na_V1.8-Cre
Het.
Homo.
Area (μm^2)
iii.
P=0.78
tdTomato-positive (%silent cold)
100
75
50
25
0
Het
Homo
B Na_V1.7 KO
P=0.38
Cells (%)
WT
Na_V1.7 KO
Area (μm^2)
C i. Sodium channel block
Oxaliplatin
Saline
1
#
35
Oxaliplatin
TTX (20 μM)
1
#
58
Oxaliplatin
anhyTTX (20 μM)
1
#
36
Cold
Cold
$\Delta F/F_0$
5
4
3
2
1
0
t = 45 s
ii.
Cold-sensing neurons (%control)
125
100
75
50
25
0
Basal
Silent
Saline
TTX
anhyTTX
iii.
Basal
Silent
P>0.99
P<0.001
P>0.99
P>0.99
P=0.002
P=0.038
$\Delta F/F_0$
4
2
0
Saline
TTX
anhyTTX
Saline
TTX
anhyTTX
D i. Sodium channel activation
Naive
Veratridine (100 μM)
1
#
53
Cold
Cold
$\Delta F/F_0$
5
0
t = 45 s
ii.
P=0.99
Area (μm^2)
600
400
200
0
Naive
Vera.
iii.
Cold-sensing cells (#)
40
30
20
10
0
Naive
Vera.
iv.
P=0.020
$\Delta F/F_0$
5
4
3
2
1
0
Naive
Vera.

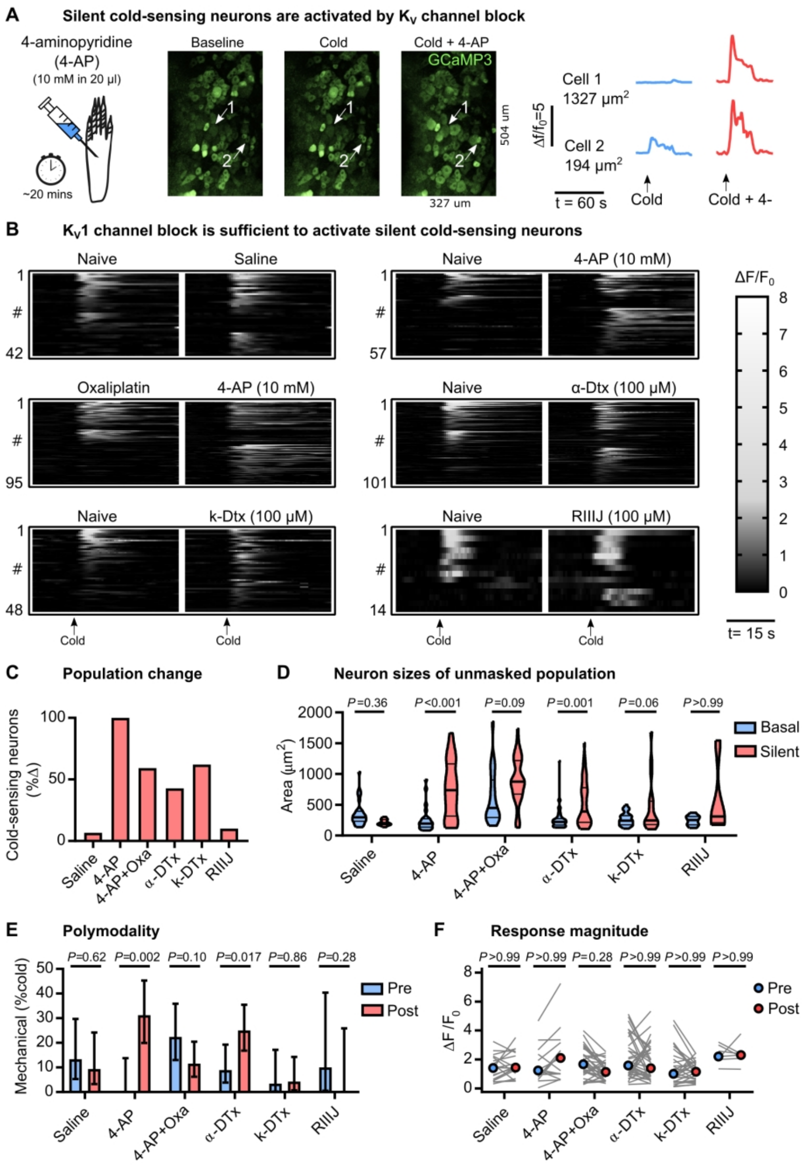
A
Silent cold-sensing neurons are activated by K_V channel block
4-aminopyridine
(4-AP)
(10 mM in 20 µl)
~20 mins
Baseline
Cold
Cold + 4-AP
GCaMP3
1
2
504 um
327 um
$\Delta f/f_0$=5
t = 60 s
Cell 1
1327 µm^2
Cell 2
194 µm^2
Cold
Cold + 4-
B
K_V1 channel block is sufficient to activate silent cold-sensing neurons
Naive
Saline
4-AP (10 mM)
Oxaliplatin
α-Dtx (100 µM)
k-Dtx (100 µM)
RIIIJ (100 µM)
1
#
42
57
95
101
48
14
Cold
$\Delta F/F_0$
8
7
6
5
4
3
2
1
0
t= 15 s
C
Population change
Cold-sensing neurons (%Δ)
100
50
0
Saline
4-AP
4-AP+Oxa
α-DTx
k-DTx
RIIIJ
D
Neuron sizes of unmasked population
Area (µm^2)
2000
1500
1000
500
0
P=0.36
P<0.001
P=0.09
P=0.001
P=0.06
P>0.99
Basal
Silent
Saline
4-AP
4-AP+Oxa
α-DTx
k-DTx
RIIIJ
E
Polymodality
Mechanical (%cold)
50
40
30
20
10
0
P=0.62
P=0.002
P=0.10
P=0.017
P=0.86
P=0.28
Pre
Post
Saline
4-AP
4-AP+Oxa
α-DTx
k-DTx
RIIIJ
F
Response magnitude
$\Delta F/F_0$
8
6
4
2
0
P>0.99
P>0.99
P=0.28
P>0.99
P>0.99
P>0.99
Pre
Post
Saline
4-AP
4-AP+Oxa
α-DTx
k-DTx
RIIIJ

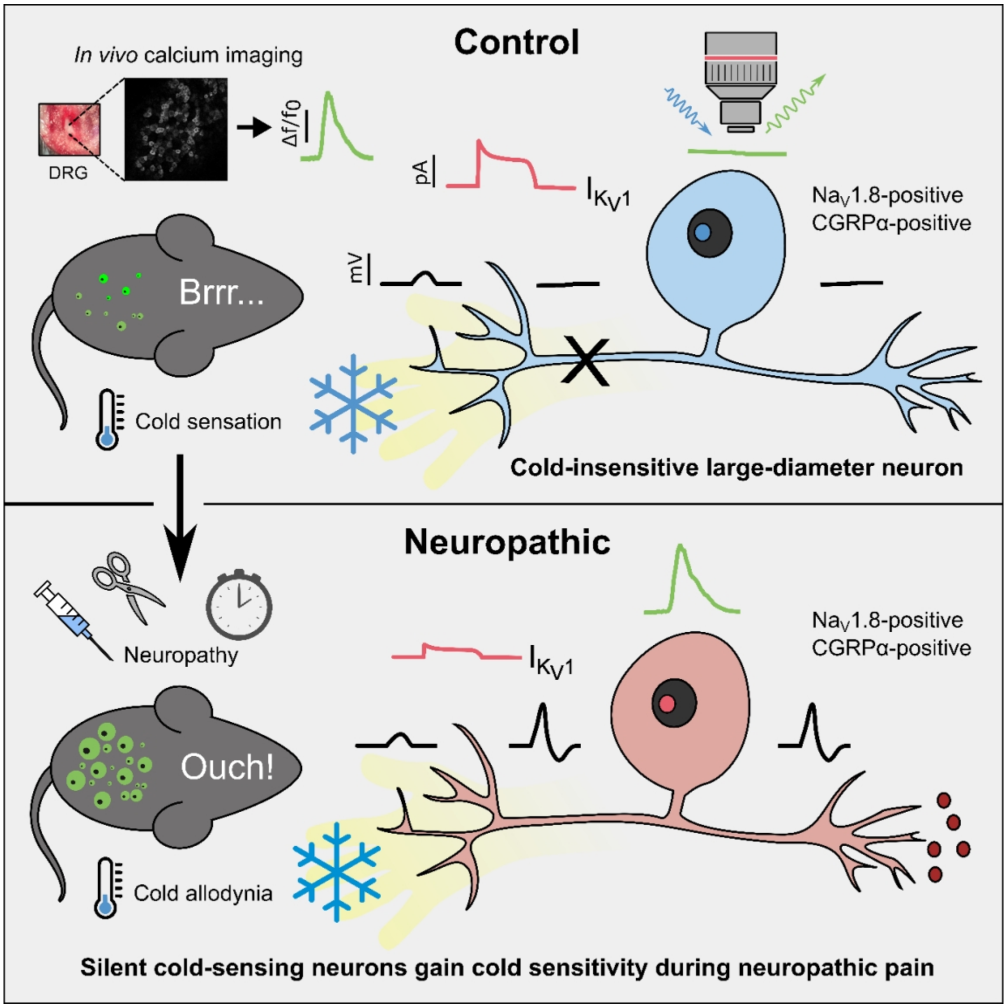
Control
In vivo calcium imaging
DRG
Δf/f0
pA
I_{Kv1}
mV
Na$_V$1.8-positive
CGRPα-positive
Brrr...
Cold sensation
Cold-insensitive large-diameter neuron
Neuropathic
Neuropathy
I_{Kv1}
Na$_V$1.8-positive
CGRPα-positive
Ouch!
Cold allodynia
Silent cold-sensing neurons gain cold sensitivity during neuropathic pain